NTNU

Norwegian University of
Science and Technology

A Wide Area Load Shedding Scheme to Prevent Voltage Instability

Jon Erik Solås

Master of Energy and Environmental Engineering
Submission date: June 2016
Supervisor: Kjetil Uhlen, ELKRAFT

Norwegian University of Science and Technology
Department of Electric Power Engineering

PROBLEM DESCRIPTION

Electric power is a cornerstone in today's society. It is the transmission system operators' responsibility to ensure that sufficient power is transferred over the transmission grid such that load demand is satisfied. With a growing load demand and increasing power transfer, the power systems are operated closer to its stability limit, putting an emphasis on the importance of properly identifying the distance to the stability limits.

The goal of this thesis is to develop an Emergency Load Shedding scheme (ELS) using voltage stability indicators. The method should detect voltage instability, and shed load as a countermeasure to regain voltage stable operation.

A literature study is carried out, where a few voltage indicators are chosen to be further studied, implemented and used in the proposed Emergency Load Shedding scheme. The study is to carried out on a model of the Norwegian power system, and implemented in an area where voltage stability previously has been a problem.

Sammendrag

I moderne kraftnett drives operasjonen nært deres stabilitetsgrenser. Små feil som linjeutfall kan derfor forårsake ustabilitet i systemet. For å unngå strømbrudd i deler av nettet, eller i nettets helhet, kreves det at tiltak blir gjort dersom det oppdages ustabilitet.

I denne avhandlingen presenteres en metode som bruker korrektive tiltak dersom det detekteres ustabilitet i kraftsystemet. Området hvor metoden er testet har en knapphet på ressurser som kan brukes for å gjenopprette stabilitet i kraftsystemet. Dette gjør at utkobling av last derfor er det eneste mulige tiltaket. Da det er store sosiale og økonomiske kostnader forbundet med utkobling av forbrukere, er målet for den presenterte metoden å koble ut minst mulig last.

Først blir fire metoder for estimering av kraftsystemets impedans, sett fra et lastpunkt, undersøkt og testet. De føste to er basert på lokale målinger ved lastpunktet, mens de resterende to metodene bruker informasjon om kraftnettet og målinger fra andre lastpunkter.

Teoremet for maksimal effektoverføring forteller at systemets impedans ikke kan være større enn lastimpedansen (Impedans-stabilitetsindeks, $ISI \geqslant 1$). Dette er blitt brukt til å sette opp et forhold mellom de to impedansene for å evaluere stabiliteten til systemet.

Indikatorens evne til å gjenkjenne tidspunktet kraftsystemet blir ustabilt er testet ved en gradvis økning i last. Når lasten er økt over sin maksimale grense skal indikatoren korrekt indikere at impedansstabilitetsindeksen er under én. Fra studiene er det kommet frem at den topologibaserte Duong-Uhlen og målingsbaserte Corsi-Taranto metoden er best i sine estimat.

Disse indikatorene er deretter blitt implementert i en foreslått metode for automatisk utkobling av last. Et utvalgt sett med laster i systemet har fått implementert indikatorer. To alternative metoder for utkobling av last er blitt testet på systemet når det er blitt utsatt for situasjoner som forårsaker ustabilitet.

Abstract

These days, power systems are operated close to their stability limit, and disturbances such as transmission line contingencies can cause the system to lose stability. If the system loses stability, countermeasures has to be taken. Otherwise, disruption in parts of, or in the whole system occurs.

In this thesis an Emergency Load Shedding scheme, (ELS) using voltage stability indicators is proposed. Due to the scarcity of available mitigation actions in the considered area in Northern Norway, load shedding is used as the only corrective action. As there are large social and economic costs associated with load shedding the goal of the ELS is to keep the amount of load shed as low as possible.

First, four methods for estimating the Thévenin impedance (system impedance) of a power system is studied and tested. Two are based on local measurement at a single substation, while the other two uses information about system topology as well. Using the stability criterion imposed by the theorem of maximum power transfer a rule for stability can be found. The load impedance divided by system impedance needs to be greater than one (Impedance Stability Index, $ISI \geqslant 1$).

The performance of the indicators is tested by a gradual load increase of a load, and evaluating if the Impedance Stability Index correctly crosses its stability limit when the system becomes unstable. From the results the topology based Duong-Uhlen and the measurement based Corsi-Taranto method showed the best performance.

Using the two best performing indicators an Emergency Load shedding Scheme is proposed. Indicators are implemented at critical nodes found through simulation. Two options for load shedding is proposed when the system becomes unstable to prevent system instability.

CONTENTS

LIST OF FIGURES

LIST OF TABLES

NOMENCLATURE

- Phasors are denoted with arrows over the variables, e.g. $\vec{V}$, and the phasors magnitudes are denoted as either $|\vec{V}|$ or only using the variable name, e.g. V.
- Matrices and vectors are shown in bold, e.g. $\mathbf{V}$ or with overline and bold if the matrix consists of impedances, e.g. $\bar{\mathbf{Y}}$.
- Matrix element identifier is in subscript, e.g. $\bar{Y}_{ij}$.
- Measured value is in superscript, e.g. V^i for the current measurement or V^{i-1} for previous measurement.

1 INTRODUCTION

1.1 BACKGROUND AND OBJECTIVE

Electric power is a cornerstone in today's society. It is the transmission system operators' responsibility to ensure that sufficient power is transferred over the transmission grid such that load demand is satisfied. With society's increasing dependency on reliable power, large efforts have been put into the research of secure power system operation. Modern power systems are operated close to their stability limit, and disturbances such as transmission line contingencies may cause the system to lose stability. If the power system loses stability, countermeasures has to be taken. Otherwise, disruption in parts of, or in the whole system occurs.

Voltage instability has been the cause of several blackouts in the last few decades [3]. In the Hellenic system, increase in power demand and a change in end-user consumption pattern was deemed the cause for two blackouts in 1994 and 2004 [4, 5]. In recent years, the Norwegian transmission system has during challenging seasons been operated in a state described as stressed. New records in power consumption and generation, with the addition of intermittent generation such as wind power, has presented challenges in both planning and operation. Therefore research into on-line monitoring tools for power system stability has become even more important, in order to maintain secure operation of the transmission grid.

The goal of a power system is to provide electric power to its consumers. If power is not delivered to the end-users, a cost is associated with not accomplishing this goal. This is often referred to as interruption cost.

In this report, interruption cost is represented by the Energy Not Supplied (ENS). If the system becomes unstable, the amount of energy not supplied increases as disruption of services in parts of, or the whole system occurs. As a consequence, partial disconnection of load can be favourable, following the loss of stability after a disturbance in the system.

To reduce the likelihood of disturbances resulting in system instability, preventive actions can be taken by the transmission system operator. These measures have a large investment cost associated with them, and during construction may cause the system to operate in stressed states, due to forced disconnections. Examples of preventive measures are construction of transmission lines and installations of Static Var Compensators (SVCs). Due to the high investment cost, preventive actions are preferable when the likelihood that that the system will be operating in an insecure state is high. Corrective countermeasures such as partial disconnection of load can also be favourable in situations where the likelihood of disturbance is rather small, but the consequences of said disturbance is high. Unlike preventive actions, there is a relatively low investment cost associated with load shedding, but a high interruption cost due to the energy not supplied to the end-users.

In this thesis, a corrective scheme is proposed using partial disconnection of load as the mitigative action. The goal is to keep the energy not supplied as low as possible, within reasonable boundaries. An Emergency Load Shedding Scheme (ELS) is proposed, using voltage stability indicators to assess the power systems stability, and actions to be taken based on the indicators assessment of stability.

1.2 SCOPE OF WORK

In this thesis voltage stability indicators based on maximum power transfer between system and load has been implemented and tested. The indicators are represented within two categories, local and topology based. After testing, the two best performing indicators are used in an Emergency Load Shedding Scheme (ELS) where demand side resources are used with the goal of reducing the interruption cost while regaining stability of the power system.

The work is done using PSS®E 33.6.0 and a model of the Norwegian power system. Time domain simulation is used as the system is subjected to large disturbances. These disturbances are non-linear, and as the dynamics involved in voltage stability often have large time constants this simulation method is a suitable choice.

Even though power system stability is a multifaceted problem, this report only focuses on voltage stability.

1.3 STRUCTURE OF THE REPORT

The report is structured as follows: In chapter 1, an overview and motivation behind the report is given, as well as a presentation of the work that has been done. Chapter 2 introduces terminology and definitions relevant to this report. In chapter 3, a brief overview of some of the aspects involved in both the statics and dynamics of voltage stability is given. Chapter 4 gives an overview of the implemented indicators, as well as the theory behind voltage stability using Thévenin impedance. Chapter 5 describes the proposed load shedding scheme. In chapter 6, the performance of the proposed indicators is tested. Chapter 7 contains a case study in the Lofot region, where the proposed emergency load shedding scheme is tested using indicators. In chapter 8, the results found in chapter 7 and to some extent chapter 6 are discussed. In chapter 9, a conclusion is given, as well as a discussion of further work to be done.

Part I

THEORY

2 TERMINOLOGY FOR ASSESSMENT OF POWER SYSTEMS

To achieve desired operation, a power system needs to remain stable. In this chapter some of the key aspects and terminology in power system stability and operation are introduced.

2.1 RELATIONSHIP BETWEEN SECURITY AND STABILITY

When assessing the overall operation of a power system, terms to indicate the power system performance is useful. Some of these terms are introduced below,

Contingency is an unexpected fault of one or more system components [6]. These components may be transmission lines, generators, capacitor banks, or other electrical elements.

Disturbances are events that are unplanned, resulting in an abnormal operating state [7].

Security is the ability a power system has to withstand disturbances. It refers to the degree of risk to keep the system operational after a contingency occurs without customer interruptions [6].

Stability has a proposed definition in [8] as,

> "*Power system stability is the ability of an electric power system, for a given initial operating condition, to regain a state of operating equilibrium after being subjected to a physical disturbance, with most system variables bounded so that practically the entire system remains intact*".

2.2 MITIGATING VOLTAGE COLLAPSE

Upon the loss of stability in a power system, it has to be taken countermeasures. Failing to do so, will lead to a disruption of services in parts of the system. Actions to counteract voltage collapse must either reduce reactive power consumption in the highly loaded area, increase reactive power by reactive compensation, or decrease system impedance. These countermeasures are most likely either saturated or not available in the area experiencing voltage collapse. This, together with the characteristic of areas where voltage instability is a problem, a high load demand and a lack of generation reduces the number of possible actions. Therefore, only load shedding is considered as the only corrective action in this report.

2.2.1 Load Shedding

Load shedding reduces the active and reactive power demand of an area, and by doing this, it reduces the reactive transmission losses. Due to the high interruption costs associated with load shedding, it should only be used as a last resort. Therefore load shedding is not initiated until the loadability limit is reached, in the proposed scheme.

2.3 POWER SYSTEM STABILITY CLASSIFICATION

Power system stability can be divided into three main categories: Rotor Angle Stability, Frequency Stability and Voltage Stability [9]. Within these, further sub classifications are defined, depending on the time constants of dynamics and type of disturbance under study. In this report, the main focus is on voltage stability.

2.3.1 Definition of Voltage Stability

The IEEE/CIGRE Joint Task Force defines voltage stability [8] as,

"*Voltage stability refers to the ability of a power system to maintain steady state voltages at all buses in the system after being subjected to a disturbance from a given initial operating condition*".

Voltage stability is further divided into two sub classifications based on the severity of the disturbance, and time scale of the dynamics involved [8].

2.3.1.1 *Large Disturbance Voltage Stability*

Large disturbances are highly non linear, and can therefore not be analysed using linearisation methods. The cause of large disturbances are often loss of generation, line contingencies or system faults [8]. Dynamics involved in large disturbance voltage stability can last from seconds to tens of minutes [9]. Large disturbances might also lead to voltage collapse, which is categorised by a sequence of events resulting in blackout, in part of, or the whole grid. In this report only large disturbances in the form of line contingencies are considered.

2.3.1.2 *Small Disturbance Voltage Stability*

Small disturbances are often caused by gradual changes in load. Small disturbance voltage stability can be studied using an linearisation approach if the dynamics of components that are highly non-linear in response are not taken into consideration [9].

In both cases, the ability of the system to maintain steady voltage after a change in the system occurs, determines if the system is voltage stable.

2.4 PHASOR MEASUREMENT UNITS

To increase the situational awareness, Statnetts research and development division has an ongoing project installing Phasor Measurement Units (PMU). By the end of 2015, they had 23 PMUs installed in the Norwegian central grid [10].

The benefits of PMUs compared to traditional SCADA systems, is the data acquisition rate. Traditional SCADA systems acquire data every 3-10 seconds. In contrast, PMUs acquire data at a rate of up to 60 times per second [11]. This is over hundred times faster, making it possible to observe the faster dynamic phenomena occurring in a power system as well.

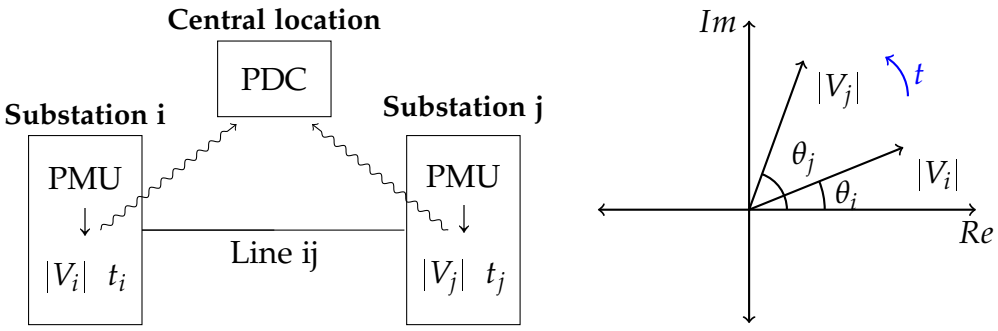

(a) Data transfer from PMUs to PDC **(b)** Output from PDC

Figure 2.1: Communication from two PMUs at different substations to a PDC

A Phasor measurement unit takes in current and voltage measurements and applies a time stamps to the measured value. The timing signals are obtained from clocks inside the substation that are synchronised using global positioning systems (GPS) [12]. The time stamped data is then sent to a phasor data concentrator (PDC), which obtains the relative angle difference for the location of PMUs in the power system. This principle is illustrated in figure 2.1.

2.5 WIDE AREA MEASUREMENT SYSTEMS

A Wide Area Measurement System (WAMS), is a monitoring system based on phasor measurement units (PMUs) [13]. The implementation of a wide area measurement system has multiple proposed usages and benefits [11]. In this report the main focus is on acquisition and processing of data in real time to assess power system stability and take action if instability is detected.

The proposed WAMS system used in this report is illustrated in figure 2.2. Here the PMU signals are sent to a a central location, preferably the central or a regional control centre where the data is processed and actions are taken based on this processed data.

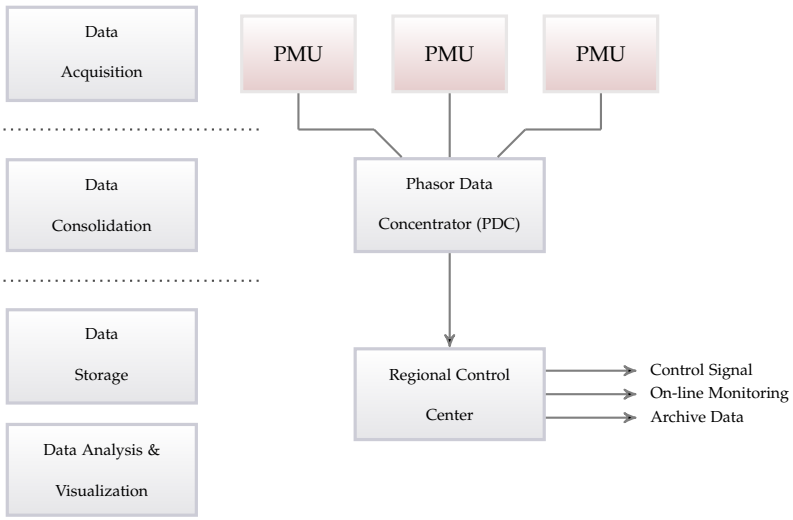

Figure 2.2: Data management and flow visualised in a Smart Grid system based on WAMS

In Norway, the transmission system operator, Statnett SF, has since 2005 developed and tested a wide area monitoring system to monitor power oscillations [11]. There is currently, as of 2016, no voltage stability monitoring system, but research is being done in cooperation between Statnett SF, NTNU and KTH. Published articles can be found in references [14, 15, 16].

2.6 REVIEW OF EMERGENCY LOAD SHEDDING SCHEMES

There are various schemes proposed for Emergency Load Shedding (ELS), to maintain voltage stable operation. These methods can be divided into two categories; local and wide area. Wide area methods measures observable quantities and gathers the data to a centralized location. In local methods the relays act based on local bus voltages or calculated stability indices [17].

Assessing stability based on voltage magnitude is proposed in many papers, and is commonly referred to as an Under Voltage Load Shedding Scheme (UVLS). In [18], stability is assessed within an area by voltage magnitude monitoring, using distributed controllers. An adaptive under voltage load shedding scheme is proposed in [19], using model predictive control. The methods using voltage magnitude have the disadvantage that they rely on an already degraded state of the power system.

A large number of methods determining the optimal amount of load to be shed have been proposed by researchers. With the increased usage of Wide Area Measurement Systems (WAMS), these methods have become closer to a reality. Using matching impedance in [20], a wide-area scheme, in order to prevent voltage instability, is proposed. Another proposed method for finding the minimal amount of load shed is the usage of sensitivities. The research into the usage of sensitivity analysis is not new in power systems, [21, 22, 23, 24]. In [24], sensitivity computations are done in order to identify when a set of load powers have passed through maximum loadability. The method has the benefit that it tries to detect the initiation of voltage instability and does not act based on the consequence.

In a emergency load shedding scheme, the time at which load shedding is initiated is also of importance. In, [25] and [26] the time between a contingency occurs and the time load shedding is initiated is analysed.

3 VOLTAGE STABILITY

3.1 LOADABILITY LIMIT

To understand the causes of voltage instability and power transfer limits in a power system, consider a simple two bus system as shown in figure 3.1. The apparant power consumed by the load can be written as,

$$P = \frac{EV}{X}\sin\theta \tag{3.1}$$

$$Q = \frac{EV}{X}\cos\theta - \frac{V^2}{E} \tag{3.2}$$

A new expression can be obtained using equation (3.1) and (3.2), and the identity $\sin^2\theta + \cos^2\theta = 1$. In this expression the angle θ can be eliminated,

$$\left(\frac{EV}{X}\right)^2 = P^2 + \left[Q - \frac{V^2}{X}\right]^2 \tag{3.3}$$

Rewriting equation 3.3 as a quadratic equation the new expression becomes,

$$(V^2)^2 + (2XQ - E^2)V^2 + X^2(P^2 + Q^2) = 0 \tag{3.4}$$

This quadratic equation has two solutions representing a high voltage and low voltage solution. Solving the equation for a given load power factor, and using $Q = P\tan\phi$ gives,

$$V = \sqrt{\frac{E^2}{2} - XP\tan\phi \pm \sqrt{\frac{E^4}{4} - X^2P^2 - XE^2P\tan\phi}} \tag{3.5}$$

Solving equation (3.5) for different values of P the PV curve is obtained as illustrated in figure 3.1.

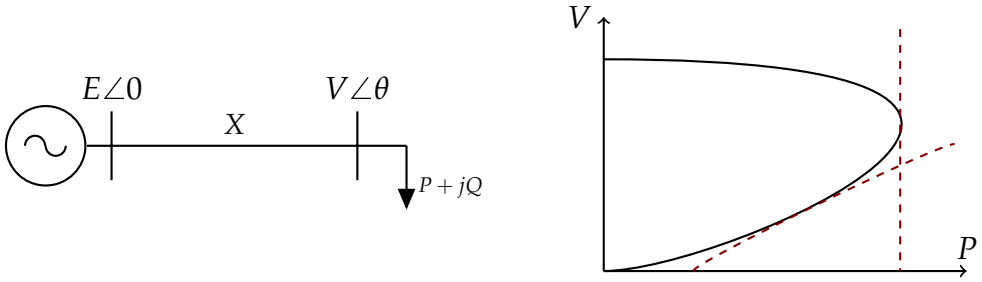

Figure 3.1: Loadability limit illustrated with a simple two bus system

This PV curve is the basis for understanding voltage stability, even though it refers to a static case, important information can be obtained from it.

The PQ relation, $\tan\phi$ determines how far the system can be loaded before the nose point is reached. A smaller or negative $\tan\phi$, will make the system less prone to voltage stability problems. One way to improve $\tan\phi$ is by installing reactive compensation at the given node.

Loadability Limit for different types of loads will not be the same. This is illustrated in figure 3.1. The vertical dashed line representing a PQ-load will reach its loadability limit at the tip of the nose point. A ZIP load represented by the curved line reaches its loadability limit below the nose point giving a higher loadability margin for the given PV curve [27].

It is important to emphasize that the load demand and consumption of power does not always correlate and is important in understanding the basis for voltage instability [9].

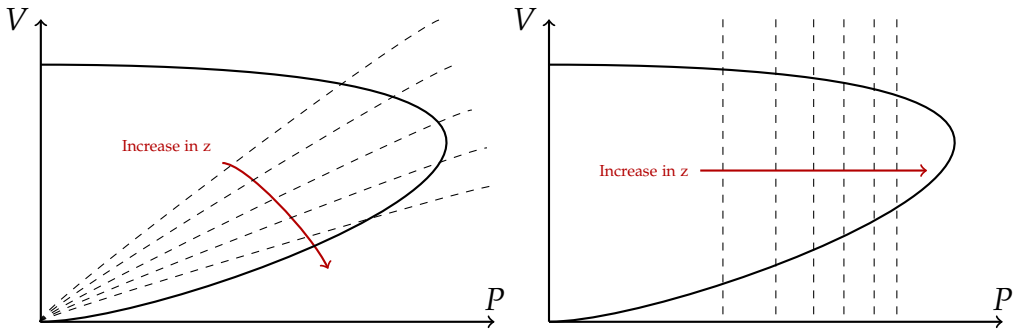

(a) Polynomial Load (ZIP) **(b)** Constant power load

Figure 3.2: Effect of an increase in load demand, z for different load types.

Consider the case in figure 3.2 where the ZIP load is increasing its demand. After a certain load demand, z, the load characteristic is below the nose point. When this point is reached we see that even though the load demand is increasing the actual power P is decreasing.

An operating point below the nose curve is theoretically feasible when considering static loads. But with the introduction of dynamic loads this no longer becomes viable. This is due to the action of self restoration as illustrated in figure 3.5. The load trying to restore itself will cause a decrease in both power and voltage, resulting in a voltage collapse.

3.2 CAUSES FOR VOLTAGE INSTABILITY

3.2.1 Transmission Line Contingencies

One of the common scenarios where voltage stability problems might occur is weakening of the network [9]. If one considers the equation for the PV curve derived in section 3.1,

$$V = \sqrt{\frac{E^2}{2} - XQ \pm \sqrt{\frac{E^4}{4} - X^2P^2 - XE^2Q}} \tag{3.6}$$

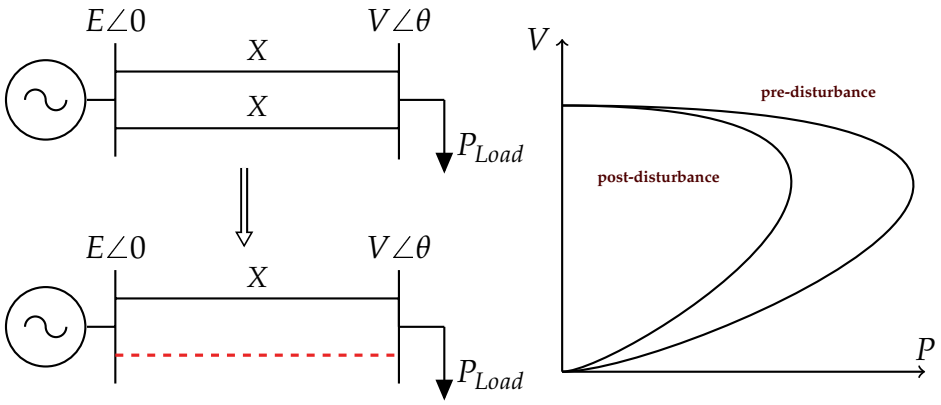

(a) Two bus system

(b) PV curves for (a).

Figure 3.3: Change in network PV curve following a line contingency

By setting $Q = 0$, assuming the load only draws real power, this reduces to,

$$V = \sqrt{\frac{E^2}{V} \pm \sqrt{\frac{E^4}{4} - X^2P^2}} \tag{3.7}$$

The maximum power transfer occur when there is only one solution to equation (3.7). This happens when the inner root expression is equal to zero,

$$\frac{E^4}{4} - X^2P^2 = 0$$

$$P = \frac{E^2}{2X} \tag{3.8}$$

If one considers the scenario given in figure 3.3 before the line contingency occur, the total reactance of the transmission line is $X/2$. After the contingency occurs, the only change in the system is a doubling in the reactance of the transmission line. As equation (3.8) for the nose point of the system is dependent on the reactance, a decrease in maximum power will occur,

$$P_{nose,prior} = \frac{E^2}{2X} \tag{3.9}$$

$$P_{nose,post} = \frac{E^2}{4X} \tag{3.10}$$

The case that is looked at in this scenario is of a radial network, but this also holds for a meshed network, as is the case for the central grid.

This is because any node can be described by its Thevenin equivalent. The change in network topology that occurs after a disturbance will therefore alter the Thevenin impedance, making the loadability limit smaller.

3.2.2 Increase in Load Demand

One way the system can become unstable is if areas with lack of generation and a weak grid gets an increase in load demand. This can happen during morning hours when people are waking up, or during cold winter days. Usually for this to happen the system needs to be in

a stressed state where a sudden increase in load demand pushes the system over its maximum loadability limit. A change in the reactive power demand will also cause a change in voltage if it is not properly compensated for.

3.3 STATIC AND DYNAMIC LOADS

For stability studies load modelling is usually split into two groups, static and dynamic load modelling. Within these two groups further division is done based on load characteristics and dynamics involved.

The loads in this report have both a static and dynamic part. The static loads are represented by ZIP-loads, and the dynamic part, is a slow restoring dynamic load.

3.3.1 Static Loads

Static loads will exhibit different behavior depending on parameters and type of the load. Three common static loads are PQ-loads, ZIP-loads and voltage dependent loads. Depending on the wanted characteristic of the load, and complexity of the system, either of these can be used.

PQ-loads are loads where P_0 and Q_0 is defined and the power remains constant with variations in voltage. This is the simplest way of modelling a load and is often used in power flow studies.

ZIP-loads is a special case of the polynomial load [9]. The ZIP-load is made up of the three components: Constant impedance (Z), constant

current (I) and constant power (P). The real and reactive characteristic of the ZIP load is given by the equations [9]:

$$P = zP_0\left[a_P\left(\frac{V}{V_0}\right)^2 + b_P\frac{V}{V_0} + c_P\right] \tag{3.11}$$

$$Q = zQ_0\left[a_Q\left(\frac{V}{V_0}\right)^2 + b_Q\frac{V}{V_0} + c_Q\right] \tag{3.12}$$

In equation (3.11) and (3.12), $a_{P,Q} + b_{P,Q} + c_{P,Q} = 1$. This ratio between the three constants will give the weighting of each term in the load. When these parameters are changed, the load characteristic changes its curvature and the response of the load. A typical ZIP-load characteristic and PQ-load characteristic for a given load demand, z, is shown in figure 3.4.

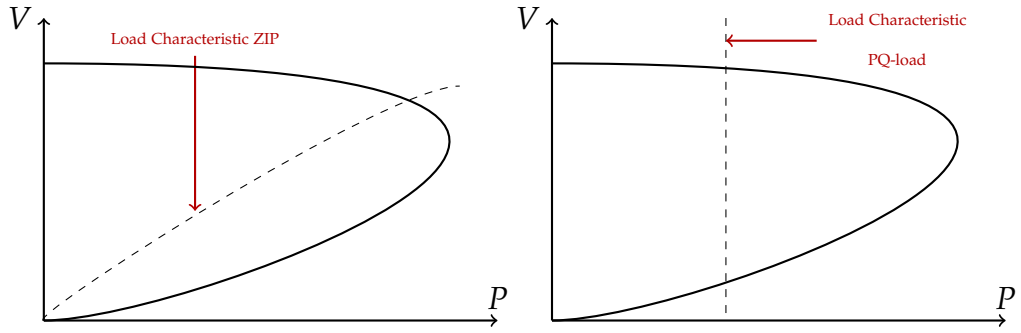

(a) Polynomial load (ZIP) **(b)** Constant power load

Figure 3.4: Load characteristics for ZIP- and PQ-loads

In this report, the weighting for real and reactive power of the ZIP-load is [28], It should be noted that the ZIP characteristic is not valid for voltages below 0.5 pu [9]. This is taken into consideration when doing simulations in PSS®E, where the function PQBRAK, changes the response of the load after a defined voltage threshold.

Real power

Constant Impedance (Z)	Constant Current (I)	Constant Power (P)
40	60	0

Reactive power

Constant Impedance (Z)	Constant Current (I)	Constant Power (P)
100	0	0

3.3.2 Dynamic Loads and Load Restoration

In certain cases, the dynamics of the load components try to restore the power after a disturbance occurs. This is referred to as load restoration. The process of load restoration may occur fast, as in the case with induction motors, or slow, as in thermostatic loads and tap changing transformers [29]. This restoration mechanism is one of the driving forces behind voltage instability.

In figure 3.5 the response of the dynamic EXTL load model is shown. A disturbance occurs, and there is a drop in voltage, causing a drop in power as well. Due to the restoration mechanism, the load power restores itself to its initial steady state value. This is in most cases ok, but if the system is in a state close to its loadability limit, voltage collapse might occur.

From a mathematical point of view a general dynamic load can be described as,

$$P = P_t(z, V, x) \tag{3.13}$$

$$Q = Q_t(z, V, x) \tag{3.14}$$

Here, x, is the load state variable, z is the load demand and V is the voltage. The state variable, x, might be rotor slip, tap changing position or other connected equipment [9]. Without any disturbances occuring, the expression reduces to,

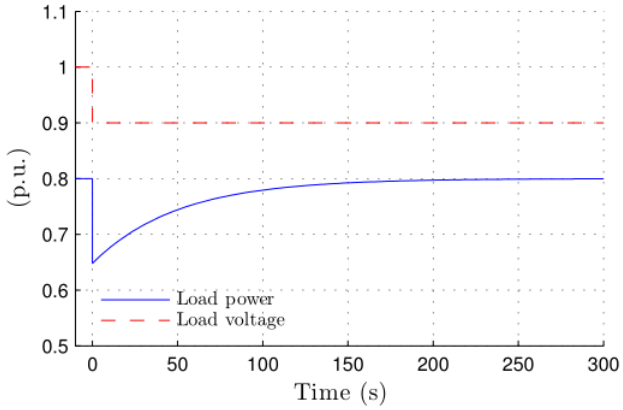

Figure 3.5: Load restoration of the EXTL model subjected to a 0.1 pu voltage drop from [1].

$$P = P_s(z, V) \tag{3.15}$$
$$Q = Q_s(z, V) \tag{3.16}$$

From equation (3.15) and (3.16) it can be seen, that in steady state, the dynamic load behaves as a static load. This is also illustrated in figure 3.6 of the EXTL load model. The dynamic load model measures the difference between P_{actual} and $P_{initial}$, and when the system is operating steady state, this equals to zero.

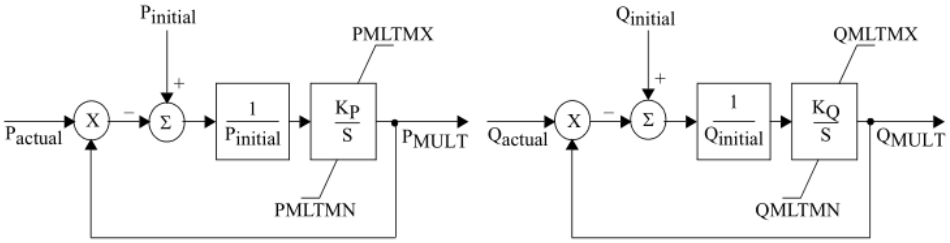

Figure 3.6: The EXTL load model from PSS®E documentation [2]

Figure 3.6 is the dynamic load model used in the case studies. Its parameters are chosen such that the load restoration process has a large time constant as shown in figure 3.5. A complete list of parameters can be found in Appendix B.1.

3.4 OVEREXCITATION LIMITERS

Overexcitation limiters (OXL) are used in generators to protect the field windings of the rotor from overheating. This is done by regulating the current flowing through the winding, so that it does not exceed a given limit. Depending on the OXL this limit may be dynamic, allowing a higher current for a certain amount, or it may be static. As shown in figure 3.7, the overexcitation limiter reduces the operational area of a synchronous generator only operating with stator current limitations. The activation of the OXL occurs faster when the generator is operating with a higher demand of reactive power.

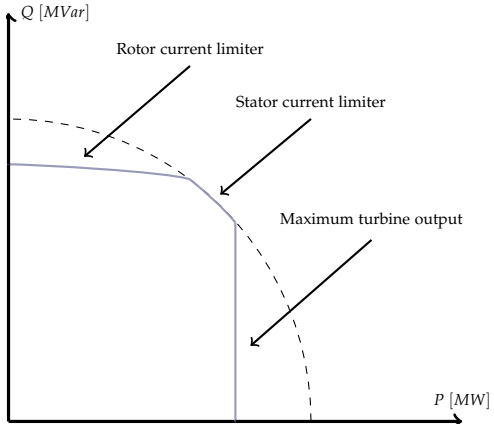

Figure 3.7: Partial capability diagram for a synchronous generator.

The block diagram of the MAXEX2 overexcitation limiter can be found in Appendix B.2 with a complete list of parameters.

3.5 OBTAINING Y_{bus}

In the topology based methods presented in section 4.6 and 4.7, $\bar{\mathbf{Y}}_{bus}$ is computed as an intermediate step when assessing voltage stability using $\bar{\mathbf{Z}}_{bus}$. In the Virtual impedance method, in section 4.7, only step 1 and 2 are used in the creation of $\bar{\mathbf{Y}}_{bus}$. The general rules used in the inspection method for obtaining $\bar{\mathbf{Y}}_{bus}$ is presented below.

Rules for obtaining $\bar{\mathbf{Y}}_{bus}$:

1. The diagonal terms of $\bar{\mathbf{Y}}_{bus}$, $\bar{Y}_{ii}$, contain the sum of all shunt terms and branch admittances connected directly to bus i.
2. The off-diagonal elements of $\bar{\mathbf{Y}}_{bus}$, $\bar{Y}_{ij}$, is the negative sum of branch elements connected between bus i and j.
3. Loads are modelled as admittances and included as shunt elements on the diagonal.
4. If considering the Thévenin impedance at bus i, load admittance at bus i is not included in $\bar{Y}_{ii}$.

The dimension of $\bar{\mathbf{Y}}_{bus}$ is dependent on number of nodes in a given power system, with n nodes the dimensions of $\bar{\mathbf{Y}}_{bus}$ is $n \times n$. A general expression for $\bar{\mathbf{Y}}_{bus}$ is presented in equation 3.17.

$$\bar{\mathbf{Y}}_{bus} = \begin{bmatrix} \bar{Y}_{11} & \dots & \bar{Y}_{1i} \\ \vdots & \ddots & \vdots \\ \bar{Y}_{j1} & \dots & \bar{Y}_{ij} \end{bmatrix} \tag{3.17}$$

3.6 TIME DOMAIN SIMULATION

As large disturbance voltage stability is non-linear, and the time constants are large, time domain simulations is a suitable simulation method

of choice.

Time domain simulations give accurate and detailed results if the power system is modelled correctly. There is a disadvantage in that it is computationally heavy, therefore simulations take a long time and it is not considered a good method for on-line assessment of voltage stability. Simplifications can be made to make simulations run faster, but in the case of long-term voltage stability, it takes time to determine the state of the system post contingency.

In this report time domain simulations are used to determine the robustness and error of indicators. For this task it is a suitable choice as you can investigate a situation that otherwise don't occur other then in the most severe cases and see how the proposed methods respond. An assumption for the validity of the result, is that the system is modelled correctly. For voltage stability studies the model provided by Statnett is not fully functional to capture all the dynamics of voltage stability, therefore additional modelling is needed.

4 ON-LINE VOLTAGE STABILITY INDICATORS

4.1 SUMMARY OF PROPOSED METHODS

In this chapter four methods for estimating the Thévenin equivalent of a power system is introduced. Two are based on local PMU measurements. The remaining two are based on system topology, and requires information about load power from SCADA and the transmission grid within the bounded area. As with the measurement based methods, PMU measurements are required at the monitored load. Additionally, measurements are required at the boundary nodes as well. In table 4.1 a brief summary of the proposed methods is given.

Table 4.1: Selected set of voltage stability indicators.

Type	Name	Index (ISI)	Stab.lim.	Ref.
Local	Delta method	$\frac{\lvert\bar{Z}_L\rvert}{\lvert\bar{Z}_{sys}\rvert}$	$ISI \leqslant 1$	[30]
Local	Corsi-Taranto method	$\frac{\lvert\bar{Z}_L\rvert}{X_{sys}}$	$ISI \leqslant 1$	[31]
Topology	Duong-Uhlen method	$\frac{\lvert\bar{Z}_L\rvert}{\lvert\bar{Z}_{sys}\rvert}$	$ISI \leqslant 1$	[14, 15]
Topology	Virtual Impedance method	$\frac{\lvert\bar{Z}_L\rvert}{\lvert\bar{Z}_{eq} + \bar{Z}_{cj}\rvert}$	$ISI \leqslant 1$	[32]

4.2 THÉVENIN EQUIVALENT

Any power system viewed from a load can be represented by the load, and a voltage source in series with an impedance, more commonly referred to as the Thévenin equivalent. This simplification holds true even if the power system represented behind the load is meshed and consists of loads, generators or other electrical components. This elegant way of representing a complex system is shown in figure 4.1.

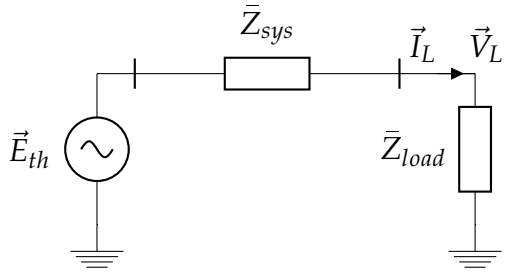

Figure 4.1: Two bus Thévenin equivalent circuit

From figure 4.1 it can be seen that the simplified circuit is easy to analyse if the circuit parameters are known. In a real power system not all the parameters are known. $\vec{E}_{th}$ and system impedance, $\bar{Z}_{sys}$ can not be directly calculated if there are components with non ideal behaviour present in the power system. In [15] it is shown that with limited generation capabilities, the evaluated Thévenin impedance, using only information about the topology gives a large deviation to the true Thévenin impedance. Therefore methods have been proposed either using consecutive measurements or information about topology together with measurements to calculate the Thévenin impedance of the system.

4.3 MAXIMUM POWER TRANSFER

4.3.1 Impedance Stability Index

The concept of *impedance stability index* (ISI) [27] is based on the theoretical maximum transfer between system and load. In [33] it is shown that the maximum power transfer is achieved when the load impedance, $|Z_{load}|$ and system impedance, $|Z_{sys}|$ are equal. From this impedance stability index (ISI) can be defined as the ratio between the two impedances where the system is considered unstable if the index is less then one.

$$ISI = \frac{|\bar{Z}_{load}|}{|\bar{Z}_{sys}|} \leqslant 1 \tag{4.1}$$

4.3.2 Power Margin

Considering the power system represented in figure 4.1 an expression for the load current, $\vec{I}_L$ can be derived,

$$\vec{I}_L = \frac{\vec{E}_{th}}{\bar{Z}_{sys} + \bar{Z}_L} \tag{4.2}$$

Rewriting as apparent power for the load, S_L and using the relation for the maximum power transfer $|\bar{Z}_{sys}| = |\bar{Z}_L|$

$$\vec{S}_{L,max} = |\bar{Z}_L||\vec{I}_L|^2 = |\bar{Z}_{sys}||\vec{I}_L|^2 \tag{4.3}$$

From this the power margin for a given load power can be found by comparing the current load power, to the maximum load power, as derived in [34],

$$\vec{S}_{L,max} = \frac{|\vec{E}_{th}|^2}{2} \frac{[|\bar{Z}_{sys}| - (Re(\bar{Z}_{sys})\cos\theta + Im(\bar{Z}_{sys})\sin\theta)]}{(\ Im(\bar{Z}_{sys})\cos\theta - Re(\bar{Z}_{sys})\sin\theta\ )^2} \tag{4.4}$$

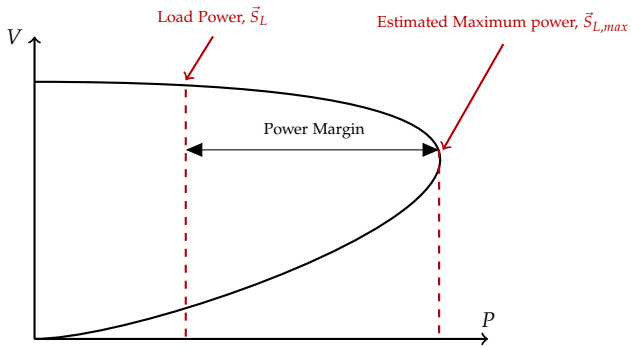

Figure 4.2: Power Margin shown on a PV-curve

It should be noted that the estimated maximum power is derived for apparent power and not real power as a PV-curve depicts in figure 4.2. The power margin is defined as,

$$margin = \frac{\vec{S}_{L,max} - \vec{S}_L}{\vec{S}_L} \times 100\% \tag{4.5}$$

4.4 THE CORSI-TARANTO METHOD

The Corsi-Taranto (CT) method from [31] is a local phasor measurement based algorithm for finding the Thévenin equivalent of a power system viewed from a monitored load. A further study is done in [35] where the proposed algorithm is tested in critical situations.

Estimating the Thévenin equivalent

The Thévenin equivalent of a power system seen from a load in the system is shown in figure 4.3. Using Kirchoff's law an expression for the load voltage can be derived:

$$\vec{V}_L = \vec{E}_{th} - \bar{Z}_{sys}\vec{I}_L \tag{4.6}$$

Here $\vec{V}_L$ and $\vec{I}_L$ are known values, while $\vec{E}_{th}$ and $\bar{Z}_{sys} = R_{sys} + jX_{sys}$ are the unknown parameters of the system.

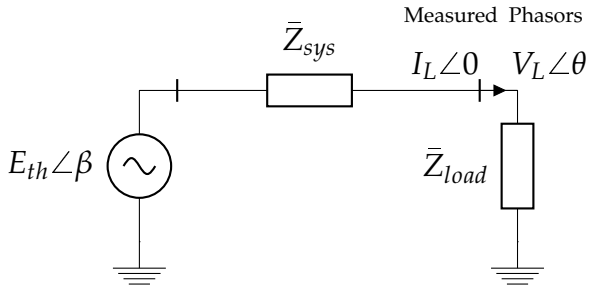

Figure 4.3: Two bus Thévenin equivalent circuit with phasor notations used in the CT-method

Using the Thévenin equivalent in figure 4.3 a phasor representation is drawn in figure 4.4. From the phasor diagram the following relationship holds:

$$\vec{V}_\Delta = \bar{Z}_{sys}\vec{I}_L = R_{sys}I_L + jX_{sys}I_L \tag{4.7}$$

$$\vec{E}_{th} = \vec{V}_L + \vec{V}_\Delta \tag{4.8}$$

In equation 4.7, $\vec{V}_\Delta$ represents the phasor from $\vec{V}_L$ to $\vec{E}_{th}$. Inserting 4.7 into 4.8 and separating the real and imaginary parts gives,

$$E_{th}cos\beta = R_{sys}I_L + V_L cos\theta \tag{4.9}$$

$$E_{th}sin\beta = X_{sys}I_L + V_L sin\theta \tag{4.10}$$

An assumption made in the method is that $X_{sys} >> R_{sys}$, therefore the assumption that $R_{sys} \approx 0$ is considered valid. In high voltage systems the R/X relationship is often in the order of $1/10$, therefore the method is less prone to errors in impedance at the highest voltage levels. The validity of the Thévenin impedance using this method is further discussed by the creators of the algorithm Corsi and Taranto in [35].

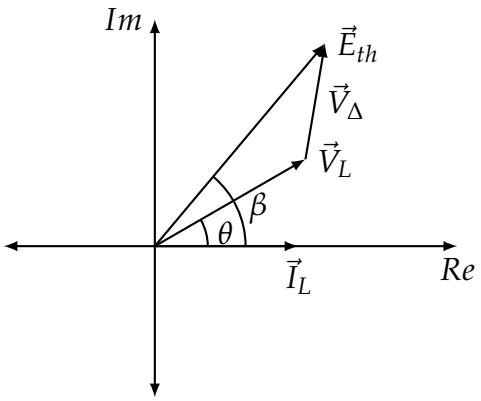

Figure 4.4: Phasor diagram for Thévenin equivalent in figure 4.3

With the assumption that $R_{sys} \approx 0$ equation 4.9 reduces to:

$$\beta = \cos^{-1} \frac{V_L \cos\theta}{E_{th}} \tag{4.11}$$

As V_L and θ are measured values the only unknown parameter is E_{th}. An initial guess of the Thèvenin voltage needs to be in agreement with the electric circuit laws, therefore:

$$V_L < E_{th}^0 < E_{th}^{nose\ point} \tag{4.12}$$

Using the approach given in [31] and arithmetic average is proposed. As the proposed approach gave varying results, a new approach for guessing the initial Thévenin voltage was used to achieve faster convergence.

$$E_{th}^0 = V_L^0 + 0.05\ (pu) \tag{4.13}$$

Even with E_{th} being inside its allowed range it should at each sampling be re evaluated to speed up the convergence of X_{th}. The algorithm also makes the assumption that E_{th} and X_{sys} are constant in the brief time frame "$i - (i-1)$", giving the requirement of a fast sampling time.

Knowing the initial values, the algorithm also needs to know which direction it should update E_{th}, and how large a step it should take to reach convergence. In brief, the value of E_{th} will be reduced when Z_L and X_{th} moves in the same direction, otherwise it will increase E_{th}.

Now that the direction is known, how large the step is should also be taken into consideration. This is calculated as follows:

$$\epsilon_E = min(\ \epsilon_{inf}, \epsilon_{inf}, \epsilon_{lim}\ ) \tag{4.14}$$

$$\epsilon_{inf} = |\ E_{th}^{i-1} - V_L^i\ | \tag{4.15}$$

$$\epsilon_{sup} = |\ E_{th}^{i-1} - E_{th}^{max}\ | \tag{4.16}$$

$$\epsilon_{lim} = |\ E_{th}^{i-1} \times k\ | \tag{4.17}$$

Here the smallest of three values are chosen as the step size for E_{th}. A pre-specified parameter k, has a large influence on how well the algorithm works. For a larger part of the convergence process ϵ_{lim} is the smallest value making the choice of k a particular difficult problem. Too large and you get an oscillatory response, and with k being too small slow the algorithm has a slow rate of convergence.

Algorithm for identifying X_{th}

---

1. Estimate initial value for E_{th}^0 using equation (4.13). Using the measured phasors for $\vec{V}_L$ and I_L together with E_{th}^0 in equation (4.11) to find an initial estimate of β^0.
2. Calculate X_{th}^0 from equation (4.10).
3. Calculate E_{th}^i according to the conditions:

   If $(\ |\bar{Z}_L^i| - |\bar{Z}_L^{i-1}|\ ) < 0$:

   If $(\ X_{th}^{i*} - X_{th}^{i-1}\ ) < 0$ then $E_{th}^i = E_{th}^{i-1} - \epsilon_E$

   If $(\ X_{th}^{i*} - X_{th}^{i-1}\ ) > 0$ then $E_{th}^i = E_{th}^{i-1} + \epsilon_E$

   If $(\ |\bar{Z}_L^i| - |\bar{Z}_L^{i-1}|\ ) > 0$:

   If $(\ X_{th}^{i*} - X_{th}^{i-1}\ ) < 0$ then $E_{th}^i = E_{th}^{i-1} + \epsilon_E$

   If $(\ X_{th}^{i*} - X_{th}^{i-1}\ ) > 0$ then $E_{th}^i = E_{th}^{i-1} - \epsilon_E$

   If load impedance is constant

$$E_{th}^{i} = E_{th}^{i-1}$$

4. Calculate β^i and X_{th}^i from equation 4.11 and 4.10.
5. Increment i and go to step 3.

PS: In the algorithm X_{th}^{i*} is an intermediate evaluation of X_{th}^i using $\vec{V}_L^i$, I_L^i with the previous value of E_{th} and β

$$X_{th}^{i*} = \frac{E_{th}^{i-1}\cos\beta^{i-1} - V_L^i\cos\theta^i}{I_L^i} \tag{4.18}$$

4.5 DELTA METHOD

The Delta method [30] is a measurement based method using consecutive measurements to estimate the Thévenin of the system viewed from a load. In this report a simplified version is implemented using only two consecutive measurements therefore eliminating the need for the least squares method.

Consider the Thévenin equivalent in figure 4.3 at a given point in time, t:

$$\vec{E}_{th}^{(t)} = \vec{V}_L^{(t)} + \bar{Z}_{sys}^{(t)}\vec{I}_L^{(t)} \tag{4.19}$$

Here we still have two unknowns in each equation $\vec{E}_{th}$, and $\bar{Z}_{sys}$. To solve this, two (or more) measurements, in this case, $t-1$, and t can be taken. Using Kirchoff's law for each of the measurements we get:

$$\vec{E}_{th}^{(t)} = \vec{V}_L^{(t)} + \bar{Z}_{sys}^{(t)}\vec{I}_L^{(t)} \tag{4.20}$$

$$\vec{E}_{th}^{(t-1)} = \vec{V}_L^{(t-1)} + \bar{Z}_{sys}^{(t-1)}\vec{I}_L^{(t-1)} \tag{4.21}$$

Even though $\vec{E}_{th}$ and $\bar{Z}_{sys}$ are still unknown we can assume that in a small time frame these values are held constant

$$\vec{E}_{th}^{(t)} = \vec{E}_{th}^{(t-1)} \tag{4.22}$$

$$\bar{Z}_{sys}^{(t)} = \bar{Z}_{sys}^{(t-1)} \tag{4.23}$$

Using this assumption of static Thévenin parameters, equation 4.20 and 4.21 can be rewritten as:

$$\vec{V}_L^{(t)} + \bar{Z}_{sys}^{(t)} = \vec{V}_L^{(t-1)} + \bar{Z}_{sys}^{(t-1)} \vec{I}_L^{(t-1)} \tag{4.24}$$

Now that $\vec{E}_{th}$ is eliminated the equation can be solved for $\bar{Z}_{sys}^{(t)}$:

$$\bar{Z}_{sys}^{(t)} = \frac{\vec{V}_L^{(t)} - \vec{V}_L^{(t-1)}}{\vec{I}_L^{(t)} - \vec{I}_L^{(t-1)}} = \frac{\Delta \vec{V}_L^{(t)}}{\Delta \vec{I}_L^{(t)}} \tag{4.25}$$

For the algorithm to work properly there has to be changes in the load current, else the impedance is not defined and problems occur. One way of counteracting this problem is to increase the sampling time, but as the sampling time increases, the assumption that $\vec{E}_{th}^{(t)} = \vec{E}_{th}^{(t-1)}$ does not hold.

Since there are always load changes in a real power system, the assumption that $\vec{E}_{th}$ is constant never holds true. This will give noise when computing the Thévenin impedance, and filtering might be required. In [30] the usage of cumulative sum filter is used to filter the estimated value.

4.6 DUONG–UHLEN METHOD

In [14], a method is presented for computing the Thévenin impedance used in on-line monitoring of voltage stability. The method uses infor-

mation about system topology and load power from SCADA to compute the Thévenin impedance at a concerned load bus in the system. To reduce the problem size and computational efforts, a bounded area within the power system, henceforth referred to as study area, is chosen where voltage stability is of concern. To model the boundary nodes, PMU measurements are required at the boundaries, as well as the load where the Thévenin impedance is evaluated from. An outline for the key steps in the method is presented below,

- Select a boundary for the load area where voltage stability is assessed.
- Simplify the load area using Gaussian elimination of $\bar{Y}_{bus}$.
- Calculate system boundary impedances.

4.6.0.1 *Topology Boundary Selection*

Voltage stability is often considered a local problem caused by high loading within a specific area where generation is scarce and the transmission grid consists of long lines. Considering voltage stability as a local phenomena, it is possible to make the problem bounded within a smaller part of the power system.

As a part of the Duong-Uhlen method, a way of determining the boundary nodes for a study area is presented in [15]. Boundary nodes should have the characteristic that if the system is close to voltage collapse, the boundary nodes should be able to maintain its voltage close to nominal value. By monitoring voltage at proposed boundary nodes when the system is close to voltage collapse the viability of the suggested boundary can be assessed. If a chosen boundary is not satisfactory, you move your boundaries further out into the system from the load area. Using the bounded area drastically reduces the problem size and hence computational efforts needed, making it more suitable for on-line monitoring of voltage stability.

4.6.0.2 *Simplification of Load Area*

With the boundary area chosen there is still no tie between generation and load if the system is meshed. Power is diverted through multiple loads along the way and flowing over different branches. In this section, a simple 7 bus system is used to illustrate the principle of reduction to get a direct tie between generation and the load bus from which the Thévenin impedance is evaluated. Consider figure 6.9, here the Thévenin is considered at bus 7, with the boundaries represented by G_1, which is modelled as an infinite bus, and G_2, a smaller generator.

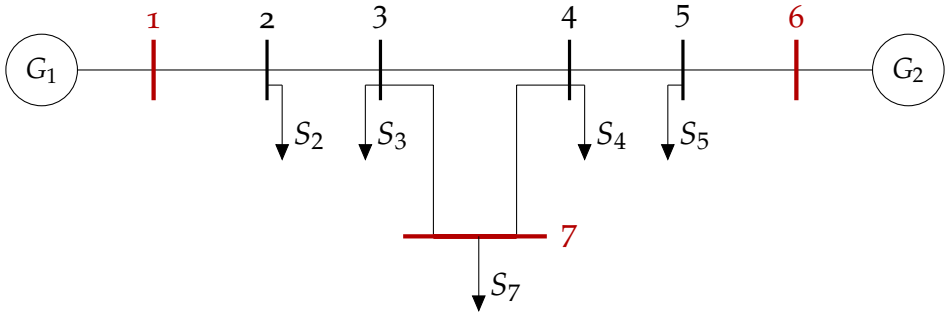

Figure 4.5: Example 7 bus system

Using a modified representation of $\bar{Y}_{bus}$ retaining boundaries and the monitored bus in the bottom right quadrant denoted as $\bar{Y}_I$ (bus 1, 6 and 7) we get,

$$\bar{Y}_{bus} = \begin{bmatrix} \bar{Y}_E & \bar{Y}_{EB} \\ \bar{Y}_{EB} & \bar{Y}_I \end{bmatrix} \tag{4.26}$$

Here $\bar{Y}_E$ is the rest of the system and $\bar{Y}_{EB}$ represents the coupling matrix between the two systems. Using Gaussian elimination technique on $\bar{Y}_{bus}$ to remove $\bar{Y}_{EB}$ below the diagonal we get [15],

$$\bar{Y}_{bus} = \begin{bmatrix} \ddots & \ddots \\ 0 & \bar{Y}_{Ieq} \end{bmatrix} \tag{4.27}$$

Here $\bar{Y}_{Ieq}$ is a dense 3x3 matrix where a direct connection between generators and the load at bus 7 is achieved. This simplified representation is shown in figure 6.10

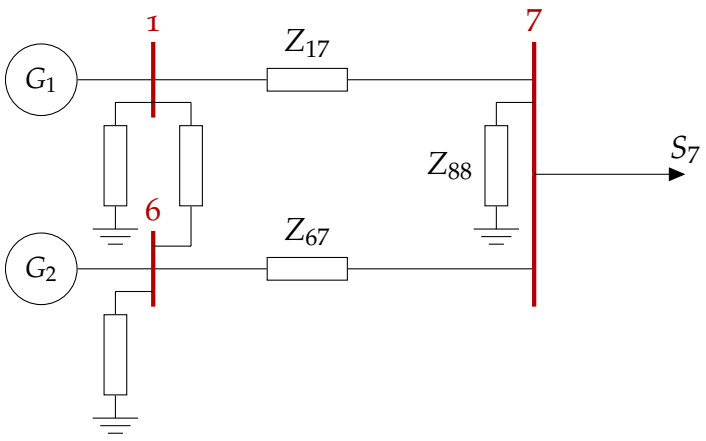

Figure 4.6: Simplified 7 bus system after Gaussian elimination

In figure 6.10 three impedances are of interest $\bar{Z}_{17}$, $\bar{Z}_{67}$ and $\bar{Z}_{77}$. As G_1 behaves as an infinite bus, $\bar{Z}_{17}$ is the constraint limiting power transfer from generator 1 to the bus 7. The impedance $\bar{Z}_67$ is the coupling impedance between bus 6 and 7, and is used to determine the virtual power flow between bus 6 and 7. This is further delved into in the next paragraph. While the unnamed impedances can be neglected in the assessment of the Thévenin impedance, the shunt impedance, $\bar{Z}_{88}$ serves an important purpose. The impedance contains information about the loading condition in the simplified sub-system and therefore should not be neglected. There are two scenarios to consider now when assessing voltage stability, either the power is flowing from bus 6 to 7 or the power flows from bus 7 to 6.

Case 1) When power is flowing from bus 7 to 6 remove bus 7 and impedances connected to this bus, a new load impedance needs to be added at bus 7, $\bar{Z}_{76new}$ which extracts the same power from bus 7. The reduces system as illustrated in figure 4.7

Case 2) When power is flowing from bus 6 to 7, $\bar{Z}_{76new}$ is modelled based on the capabilities of G_2. From [15] we obtain an expression for the new impedance. The reduces system as illustrated in figure 4.8.

$$\bar{Z}_{76new} = \frac{E_{th}^2}{4P_{max}} + j\frac{V_2^2}{4P_{G2}} \tag{4.28}$$

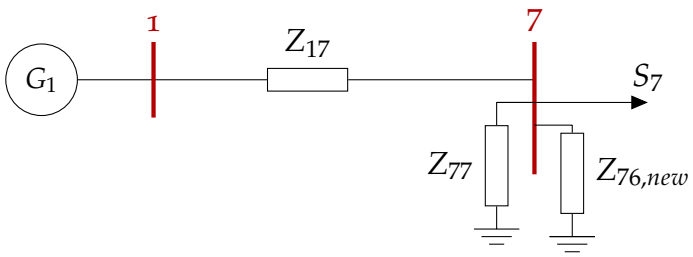

Figure 4.7: Equivalent circuit with power flowing from bus 7 to 6

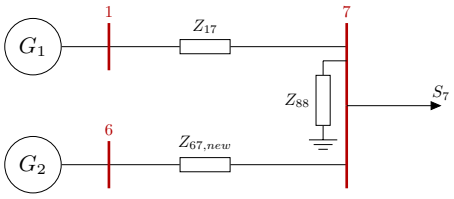

Figure 4.8: Equivalent circuit with power flowing from bus 6 to 7

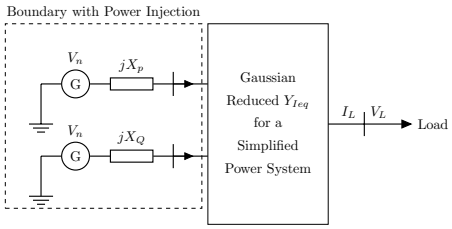

Figure 4.9: Generator model when power is flowing from 6 to 7

It should be noted that this method is not needed when generators contribute equally on the boundaries. With a limiting generator as G_2, system modifications have to be made as the transmission line no longer acts as the limiting factor in power transfer.

4.7 VIRTUAL IMPEDANCE METHOD

Figure 4.10 shows a multi-port representation [36] of a power system distinguishing between load and generator buses. This power system model consists of m generator buses, n load buses and tie buses. The power system can be described by its injected currents in equation 4.29,

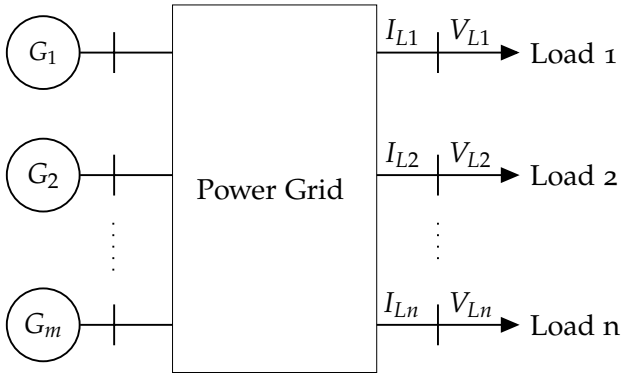

Figure 4.10: Multi-port power system model

$$\begin{bmatrix} -\vec{I}_L \\ 0 \\ \vec{I}_G \end{bmatrix} = \begin{bmatrix} \bar{Y}_{LL} & \bar{Y}_{LT} & \bar{Y}_{LG} \\ \bar{Y}_{TL} & \bar{Y}_{TT} & \bar{Y}_{TG} \\ \bar{Y}_{GL} & \bar{Y}_{GT} & \bar{Y}_{GG} \end{bmatrix} \begin{bmatrix} \vec{V}_L \\ \vec{V}_T \\ \vec{V}_G \end{bmatrix} \tag{4.29}$$

where the subscripts L, T and G are respectively for load, tie and generator. From figure 4.11 the load voltage can be written as,

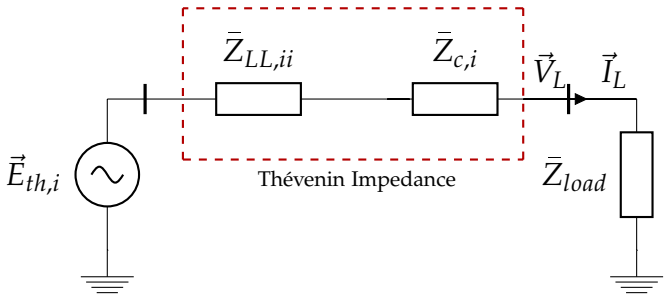

Figure 4.11: Thévenin representation for the virtual impedance method

$$\vec{V}_L = \vec{E}_{open} - \bar{Z}_{LL}\vec{I}_L \tag{4.30}$$

Here $\vec{E}_{open}$ and $\bar{Z}_{LL}$ is calculated as [37],

$$\bar{Z}_{LL} = (\bar{Y}_{LL} - \bar{Y}_{LT}\bar{Y}_{TT}^{-1}\bar{Y}_{TL})^{-1} \tag{4.31}$$

$$\vec{E}_{open} = \bar{Z}_{LL}(\bar{Y}_{LT}\bar{Y}_{TT}^{-1}\bar{Y}_{TG} - \bar{Y}_{LG})\vec{V}_G \tag{4.32}$$

From this equation 4.30 can be written as,

$$\vec{V}_{Li} = \vec{E}_{open,i} - \bar{Z}_{LL,ii}\vec{I}_{L,i} - \sum_{j=1,i\neq j}^{n} \bar{Z}_{LL,ij}\vec{I}_{L,j} \tag{4.33}$$

The third term in equation 4.33 represents the effect of other loads on the jth load when assessing the stability index.

$$\bar{Z}_{eq,i} + \bar{Z}_{c,i} = \bar{Z}_{LL,ii} + \sum_{j=1,i\neq j}^{n} \bar{Z}_{LL,ij}\frac{\vec{I}_{L,j}}{\vec{I}_{L,i}} \tag{4.34}$$

$$Index = \frac{|\bar{Z}_L|}{|\bar{Z}_{eq,i} + \bar{Z}_{ci}|} \tag{4.35}$$

4.8 IMPLEMENTATION DETAILS OF ON-LINE INDICATORS

Here is a brief overview of implementation process of different indicators and challenges encountered. The implementations are done using MATLAB with simulation results from PSS®E. Every measured value is taken at the 130 $[kV]$ side of the transformers. Therefore loads are an aggregate of transformer impedance, the actual load and in some cases shunt elements connected at the secondary side of the transformer.

From PSS®E apparent power (3-phase) and voltage magnitude measurements (V_{LL}) are obtained in pu. The reason apparent power is taken as a measurement and not current directly is that in PSS®E there is no current channel. Therefore using the measured apparent power and voltage magnitude, load current needs to be obtained using ohms law:

$$\vec{S}_{3\phi} = 3\vec{V}_{1\phi}\vec{I}^{*}_{1\phi} = \sqrt{3}\vec{V}_{LL}\vec{I}^{*}_{LL} \quad [pu] \tag{4.36}$$

Rewriting ohms law assuming a star connected load an expression for $\vec{I}_{1\phi}$ can be obtained. As $\vec{V}_{LL}$ is considered the reference there is no

voltage angle, $\vec{V}_{LL} = |V_{LL}|$. From this we get an expression for the current:

$$I_{LL}\angle\theta = \frac{(P_{3\phi} + Q_{3\phi})^*}{\sqrt{3}|V_{LL}|} \quad [pu] \tag{4.37}$$

As the topic studied is voltage stability loads are represented as impedances compared to power subtractions as in the case for power flow studies. An expression for impedance can be obtained directly from apparent power and voltage magnitude,

$$\bar{Z} = \frac{|V_{LL}|^2}{S^*_{3\phi}} \quad [pu] \tag{4.38}$$

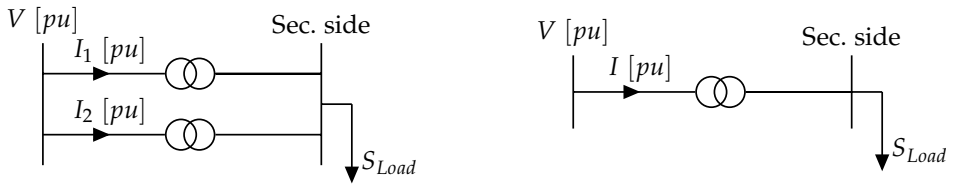

(a) Two transformers in parallel towards a load bus

(b) One transformer connected to a load bus

Figure 4.12: Illustration of measurement taken in the implementation of indicators

In the case of two transformers in parallel as shown in figure 4.12, KCL is used to get the current for the total load.

4.8.1 Corsi-Taranto Method

The CT Method uses an iterative approach for determining the Thévenin equivalent parameters. The method starts from an initial starting point defined in the implementation, and converges towards a steady state value. This initialization process only happens when the algorithm is commissioned, but extra care should be taken if the approach is used in a ELS, as false instability triggers can happen during the convergence process. In operation and convergence, the parameter, k from equation 4.17 is of great importance. The algorithm, when evaluating the smallest value of the three, often chooses equation 4.17. A larger k gives

faster convergence, while with a smaller k the rate of E_{th} and therefore X_{th} decreases. If k is chosen too large, the other two terms may become smaller, thus changing the algorithm's decision making. Therefore, the value of this parameter must be chosen carefully. From testing, values of k in the range of 0.0001 to 0.0005 gave good results.

4.8.2 Delta Method

The Delta method takes the difference of two consecutive current and voltage measurements to obtain an estimate of the Thévenin Impedance. To reduce noise, filtering is a requirement, which in this report was solved by the requirement of a minimal amount of change between two consecutive measurements being introduced. To reduce large spikes in the result, a requirement for change was set on the current, $\Delta\vec{I}_L^{(t)} > 0.001 - 0.000001$. If this requirement was not fulfilled, $\bar{Z}_{sys}^{(t)} = \bar{Z}_{sys}^{(t-1)}$. The large variation of the minimum change level for $\Delta\vec{I}_L^{(t)}$ is due to the variation of scenarios the algorithm has been tested on.

4.8.3 Doung-Uhlen Method

The general theory for the Doung-Uhlen Method is presented in section 4.6. In discussion with the author of the paper, a simplified version of the method is implemented in this paper. The implementation details and outline of the method are presented in this section.

4.8.3.1 *Choice and Modelling of Boundary Area*

In figure 4.13, the system reduction used in this report is shown. The boundary is chosen based on model behaviour at the given boundary nodes. B_1 and B_2 have generation capabilities for keeping the voltage near nominal value, while B_3 is connected to a strong 400 kV grid with a larger SVC connected, therefore exhibiting the same behaviour. Multiple boundary areas have been tested, with all using the same principle as discussed in section 4.6.0.1. To model the boundaries, a load

increase was introduced at node 1, and by observing at the moment of maximum loadability if $|\bar{Z}_{L1}| = ||\bar{Z}_{sys}|$, adjustments were made to the boundary impedances. Measurements from other loads are also re-

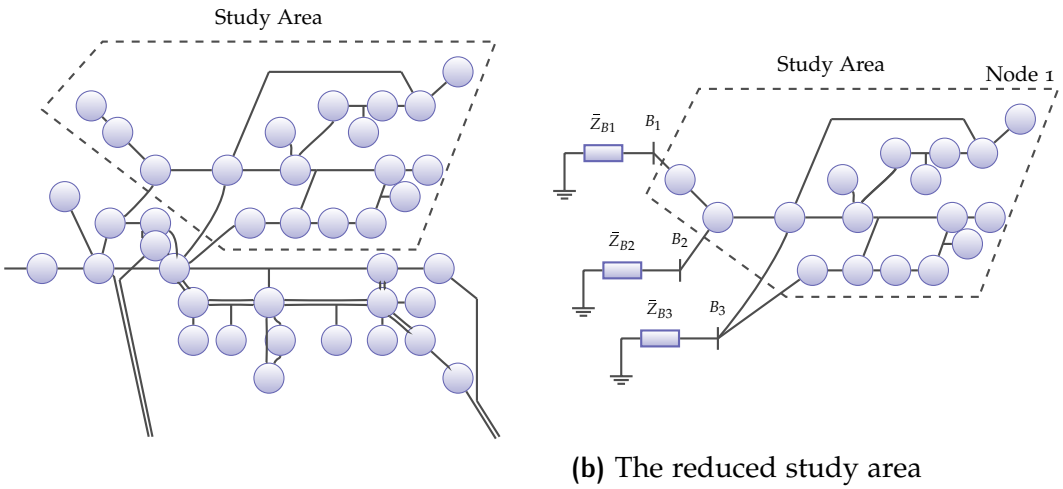

(a) Prior to reduction

(b) The reduced study area

Figure 4.13: Reduction of a larger power system to a smaller study area.

quired and if a given load does not serve as a indicator node, measurements are obtained from SCADA and are assumed updated every 10 seconds. At the indicator nodes and boundaries it is assumed that PMU measurements are available with fast sampling time. A brief overview of the implementation steps and on-line monitoring of the proposed simplified model is given below,

---

Outline of the Simplified Duong-Uhlen method for computing $\bar{Z}_{ii}$

---

1. Select a boundary for the area where voltage stability is assessed.
2. Create $\bar{\mathbf{Y}}_{bus}$ based on current topology of the considered study area without adding shunt elements
3. From SCADA compute load admittance based on current and voltage measurements.

4. Add boundary admittances and load admittances to their respective diagonals in $\bar{\mathbf{Y}}_{bus}$.
5. Invert $\bar{\mathbf{Y}}_{bus}$ to obtain $\bar{\mathbf{Z}}_{bus}$.
6. Compute $\mid \bar{Z}_{L,ii} \mid$ and compare to $\mid \bar{Z}_{bus,ii} \mid$. With new measurements go back to step 3.

Notes:

- The node with an indicator does not have its value included in $\bar{\mathbf{Y}}_{bus}$.
- PMU measurements are required at boundary nodes and the indicator node.
- Other load nodes should calculate admittance based on SCADA measurements.
- If a transmission line contingency occurs within boundary area, go to step 2.

4.8.4 Virtual Impedance Method

The boundary selection used in the implementation of the virtual impedance method is the same as with the Doung-Uhlen method. The key difference between the two is that the boundaries in the Virtual Impedance Method are represented as generators as illustrated in figure 4.10. In the structuring of the admittance matrix from equation 4.29, these buses were considered as generator buses. In B_1 and B_2 the respective generators at the buses were used, while at B_3 the power flowing into to the region is assumed to represent the generator. The chosen area with generators are illustrated in figure A,

Measurements from other loads are also required and if a given load does not serve as a indicator node, measurements are obtained from SCADA and are assumed updated every 10 seconds. At the indicator nodes and generators it is assumed that PMU measurements are avail-

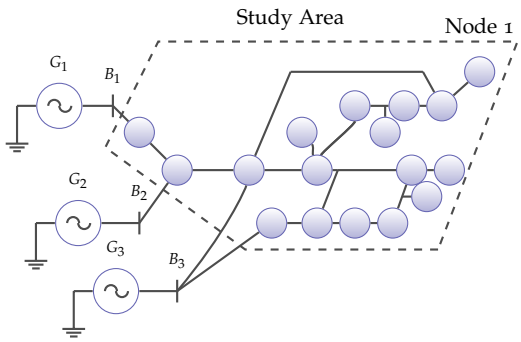

Figure 4.14: Study system implementation using the virtual impedance method

able with fast sampling time.

Part II

PROPOSED EMERGENCY LOAD SHEDDING SCHEME

5 DESCRIPTION OF PROPOSED EMERGENCY LOAD SHEDDING SCHEME

In this report Indicator Stability Index (ISI) is used to assess if the system is stable. If the Thévenin Impedance is calculated correctly it is a simple and elegant approach of assessing how far a given loading point is from the loadability limit. Drawbacks using indicator stability index is that even though the margin to maximum loadability is calculated, there is no information about when or if voltage collapse might occur. Therefore the usage of a corrective scheme where mitigation actions are initiated automatically if the indicators crosses a predefined threshold is proposed.

The considered study area in this report is categorized by high loading, lack of generation and long 130 $[kV]$ transmission lines. Further the area has few mitigation actions or they are already saturated in situations where voltage collapse is approaching. Taking this under consideration a Emergency Load Shedding (ELS) scheme is is found to be a suitable choice over a System Integrity Protection Scheme where alternative resources are used before load shedding is initiated.

This chapter describes a emergency load shedding scheme that evaluates voltage stability based on indicators placed a critical nodes in the system.

5.1 OVERVIEW

An overview of the proposed algorithm for the emergency load shedding scheme is presented in figure 5.1. Indicators are implemented at critical nodes and they system state is assessed based on the indicator values. The states are represented as normal, critical and collapse.

At the critical level power system operators are warned that given indicators indicate that the impedance stability index is below a certain threshold. The proposed algorithm does not tell the operator what to do, it is assumed that the operator makes the decision of what is to be done to restore the system.

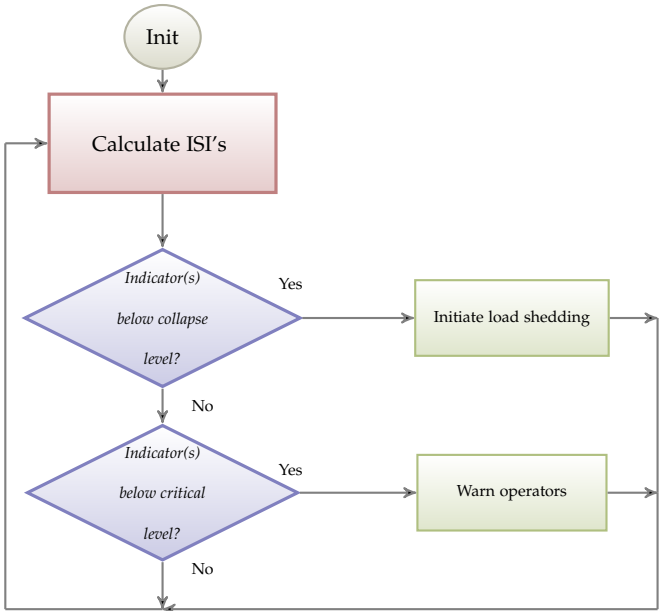

Figure 5.1: Flowchart for the proposed emergency load shedding scheme

At the critical level load shedding is initated after a time delay. This delay is introduced as short circuits may occur giving large spikes in the indicators assessment of voltage stability. As there are fast and slow dynamics involved their are two conditions that can be met to initate load shedding. One involves a fast deterioration of system state, while

the other takes into account the slower dynamics giving more time to assess stability.

5.2 PRE-COMMISSIONING CONSIDERATIONS

5.2.1 Selection of Indicators

A critical part of the emergency protection scheme is the choice of voltage stability indicators. Detailed analysis and testing should be done prior to implementing the ELS. The robustness of the indicator for different types of disturbances as well as steady state operation needs to be tested exhaustively. As voltage collapse does not occur often, the effectiveness of a given indicator when the system loses stability needs to be tested using simulation software, preferably time domain simulation. Here care needs to be taken of the correctness of the model compared to the real study system where the indicator is implemented.

5.2.2 Determining Critical Alarm Levels

The proposed emergency load shedding scheme consists of three states; normal, alert, critical. A system will in all but the most severe cases be in the normal state. A brief overview of the states are given in table 5.1. The levels of the states are based on simulations. In [20] load shedding is initiated at an ISI level less than 2, this is considered to conservative in this report.

5.2.3 Determining Amount of Load Shed

In the proposed scheme load shedding is available at the nodes where indicators are placed. For the proposed scheme to be realisitc considerations has to be taken into limits of load shedding. Any load has the possibility of shedding 10 $[MW]$. Load shedding is always initiated on

Table 5.1: Emergency Load Shedding scheme state description

State	Impedance Stability Index	Action
Normal	ISI $\geqslant$ 1.4	No actions taken
Critical	1.4 > ISI > 1.0	Warn system operators
Collapse	ISI $\leqslant$ 1.0	Initiate load shedding if: ISI $\leqslant$ 0.9 ISI $\leqslant$ 1.0 minimum 4 $[s]$

the load where the indicator crosses over to the collapse state first, if the system does not regain stability after shedding 20 $[MW]$, load shedding is initiated on the load that crossed into the collapse state as the second. To find the amount of load to be shed two methods are tested in this report.

Method 1)

Shed 10 $[MW]$ and assess stability. Post shedding, if the indicators evaluates to $ISI \leqslant 1$ within a time span of 5 minutes, another 10 $[MW]$ should be shed instantly. Repeat until voltage stable operation.

Method 2)

Evaluate ISI and measure load power before load shedding is initiated and using the information calculate the amount to be shed

$$P_{shed} = P^i \times (1 - ISI^i) \times k \tag{5.1}$$

A consideration that needs to be taken into consideration using this approach is the load power changing after contingencies due to characteristic of the load. This is illustrated in figure 5.2

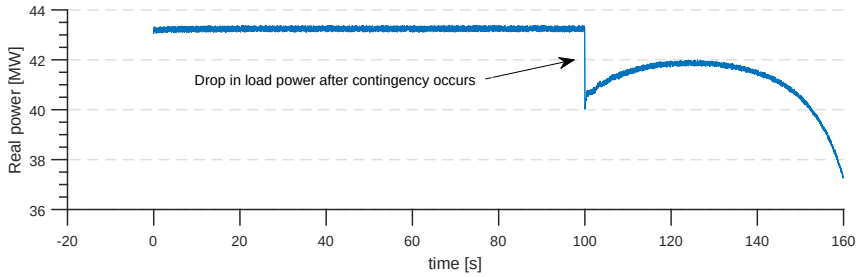

Figure 5.2: Load power after a line contingency occurs

The constant k is a correctional factor implemented after finding that the original approach $P_{shed} = P^i \times (1 - ISI^i)$ did not give satisfactory results. The constant k is suggested as 4 in this report. It should be noted if P_{shed} is always rounded up to the nearest possible amount of load to be shed. Which in this report is either 10 or 20 $[MW]$.

5.3 OPERATIONAL DETAILS

In operation the state of the impedance stability indexes is updated continuously. Based on the rate of data acquisition and computational time of impedance stability index the algorithm monitors the stability by comparing to the predefined state values set during commissioning of the system. Using the proposed values set in this report would look like

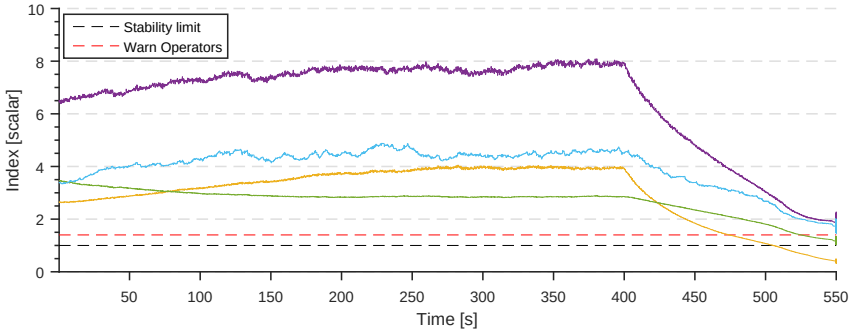

Figure 5.3: Predefined warning and load shedding levels visualised.

Part III

RESULTS AND DISCUSSION

6 INDICATOR PERFORMANCE ASSESSMENT

In this chapter, the performance of the different indicators and the ability to indicate voltage collapse at the correct node is assessed. For all the indicators, a gradual load increase is introduced at Node 1 in the study area. The load is increased until the load reaches its loadability limit and then further increased until voltage collapse. The reason voltage collapse does not occur at the loadability limit is due to the ZIP characteristic of the load, giving it a loadability limit that is below the nose point. For this report it is assumed that the load reaches its loadability limit at the nose point. This assumption is valid as load restoration is present, making operating points below the nose point unstable. For a correct assessment of instability, the Indicator Stability Index (ISI) should cross the value one when the maximum loadability is reached.

For steady state performance of the measurement based methods, ambient load noise is added to simulate the constant small load changes occurring in power systems. This measurement noise is also a requirement for the measurement based methods to work, as their convergence is dependent on a change between consecutive measurements.

The study in this chapter is done on a model of the Norwegian power system provided by Statnett SF. Due to restrictions on the data, care is taken in the presentation of results and only publicly available information is presented. Nodes that are of relevance are represented by numbers instead of there real names, and no critical model data is presented.

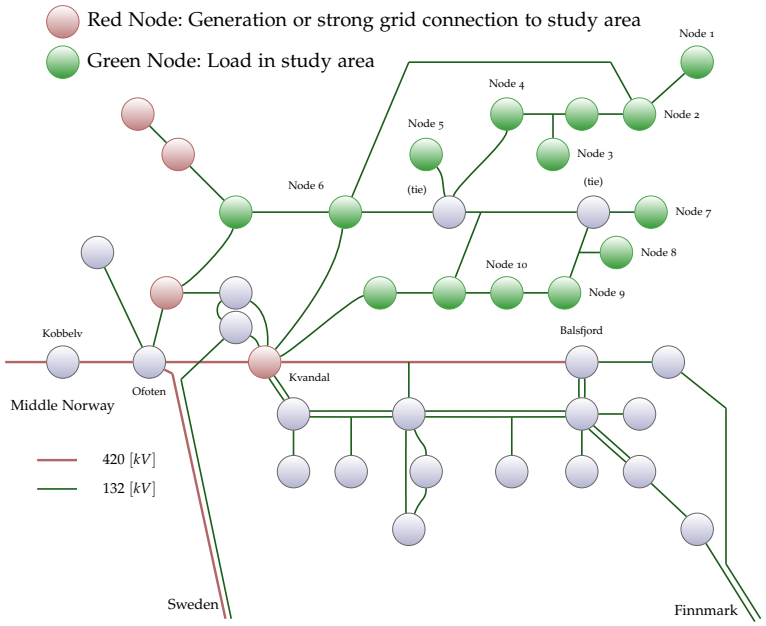

Figure 6.1: Indicator placements in the study area

For reference the reader should refer to node numbering in figure 6.1 when reading this chapter. Some loads are not part of the indicator testing. This is a choice based on either the size of the concerned load or the assessment that the nodes were not prone to voltage instability. Some additional details about the modelling relevant to the study system in question is introduced.

6.1 OPERATING SCENARIO

The basis scenario for the steady state operation in the provided model is a high load scenario for a typical winter day in Norway. As of early 2016 the region has been reinforced by the addition of capacitor banks and an SVC [38]. These new additions are not part of the study done in this thesis. This is considered a valid assumption as components may fail or need maintenance, therefore a weakened state of the power system might occur.

In the operating scenario, the Northern Norway region is importing 550 $[MW]$ from Middle Norway and exporting 440 $[MW]$ to Sweden due to a high load demand. Out towards the Lofoten region there is a load demand of 340 $[MW]$, and no generation. Further North there is a an export of 110 $[MW]$. This means that the region generates enough power to support its own demand during the day.

6.2 MODEL DESCRIPTION AND ASSUMPTIONS

6.2.1 Disconnection of Small Scale Generation

An assumption made in this report is that small scale generation located around the study region is disconnected. This is considered a valid assumption as the generators are modelled closer in the model than how they are located in reality.

6.2.2 Overexcitation Limiters

Most of the larger generators in the model have pre modelled overexcitation limiters. This means that only a few generators will need additional modelling, when operating under the assumption of disconnection of small-scale generation. To model the overexcitation limiters, the MAXEX2 model from the PSS®E model library is used. Parameters can be found in Appendix B.2.

6.2.3 Load Modelling

In the original load modelling, static ZIP load models are used. To model the response of tap changing transformers and self restoring loads, the EXTL load model from the PSS®E library is used. The parameters are chosen such that the load restoration has a large time

constant, resulting in a restoration process happening over a long time span. The load model is applied to all the loads in Northern Norway, but Sweden and Finland are still considered to be ZIP loads. In the scenarios where a gradual load increase is introduced at node 1 the load is only considered a ZIP load.

6.3 CORSI-TARANTO METHOD

6.3.1 Steady State Performance

A requirement for convergence of the CT-method is ambient load noise. Once convergence is reached, the algorithm evaluates the impedance between measurements as constant, as long as no change in load is measured. The direction of reactive power flow has been found to have a major impact on the convergence of the method. In figure 6.2, node 1 is presented in two scenarios, one where the load is capacitive and another where the load is inductive.

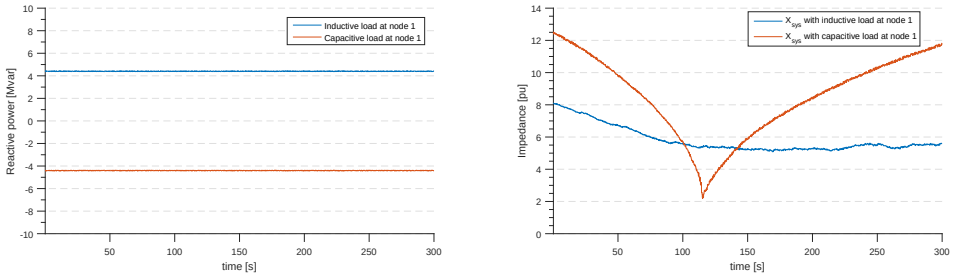

Figure 6.2: Convergence of the CT-method when implemented on a capacitive and inductive load

In the model, the load at node 1 has capacitor banks connected to the 22 $[kV]$ subsystem, causing the aggregated load seen from the 132 $[kV]$ side to be capacitive. As all measurements are assumed at the high voltage side of the transformer, this is not an uncommon occurrence in the given study area. From figure 6.2 it can be seen that capacitive loads do not converge to a steady state for the CT-method. Even though

the CT-method does not converge to a steady state, it predicts voltage collapse rather well. This is found to be a result of the load changing reactive power demand from capacitive to inductive when the system is close to voltage collapse. A solution to the problem is considering all the loads as inductive by taking the absolute value of the angle between current and voltage, when current is considered the zero reference as in the phasor diagram in figure 4.4. To test the validity of the assumption that all loads can be considered inductive, a test is conducted, shown in figure 6.3.

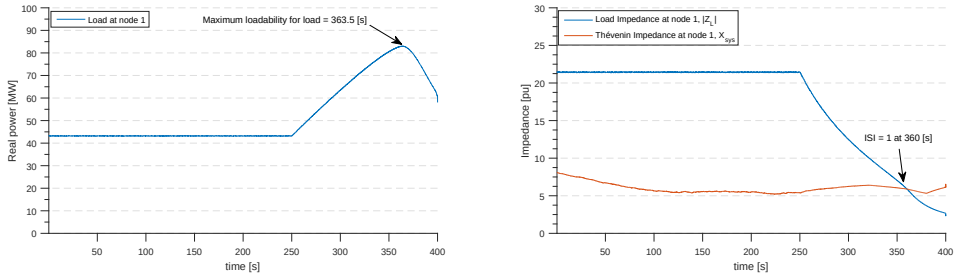

Figure 6.3: Indicating maximum loadability using the CT-method

Figure 6.3 shows a scenario with ambient load noise for 250 seconds followed by a gradual load increase at node 1. It can be seen that the assumption that the load can be considered inductive holds. At $t = 200 - 250\ [s]$, the system impedance lies between $5.2 - 5.5\ [pu]$. As there is no change in system state other than a gradual load increase, the system impedance should stay constant through the simulation and cross the loadability limit at $t = 363.5\ [s]$. When the load start increasing, the system impedances increase slightly, therefore predicting instability 3.5 seconds earlier than the actual maximum loadability. As the method assumes $R_{th} = 0$, a slight deviation is the be expected, but the overall performance is within acceptable limits.

To assess the performance of the indicators at other loads in the study area, the indicators are implemented at node 1 to node 10. The convergence of all the ten nodes using only ambient load noise is shown in figure 6.4.

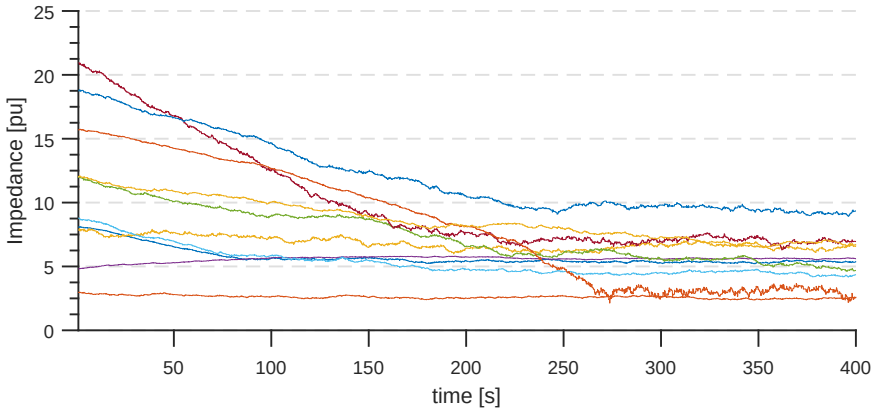

(a) Convergence process of X_{sys}

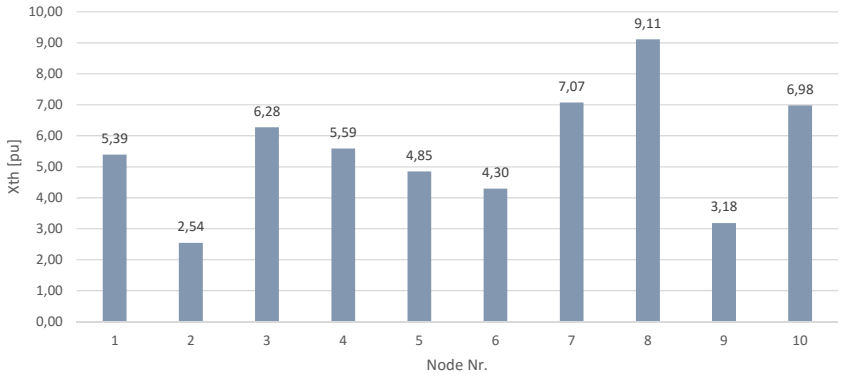

(b) X_{sys} after convergence at $t = 350$ $[s]$

Figure 6.4: Convergence of Thévenin impedance, X_{sys} for node 1-10 using CT-method

As the inital values of the indicators are not finely tuned, the convergence time of X_{sys} in figure 6.4 varies, but after 300 seconds steady state is obtained for the Thévenin impedance estimates. The steady state value of the Thévenin impedance for the different nodes can be found in the bar chart. The results for all the nodes except node 9 are within reason. The reason why X_{sys} at node nine converges to a lower than expected system impedance is not known, but a reason might be that

there is negligible reactive power flowing to the the load, or in other words, that the angle between load and current is ≈ 0.

Using the same scenario as in figure 6.3, but with ambient noise for 400 seconds prior to load increase, the ability for the indicators to predict voltage collapse at the correct node can be studied.

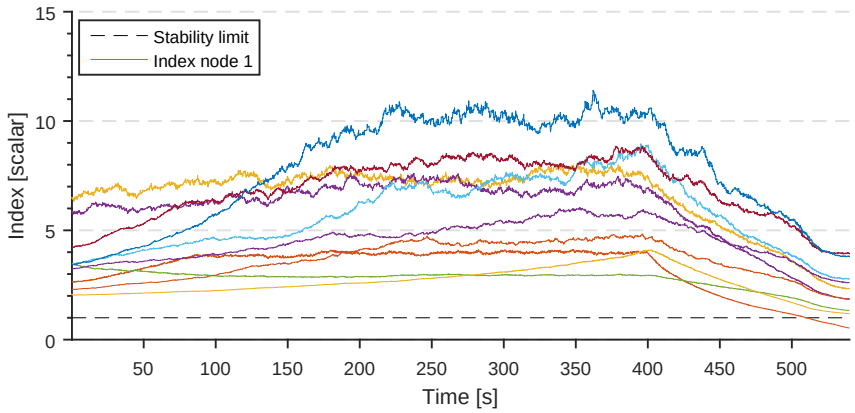

(a) Index values

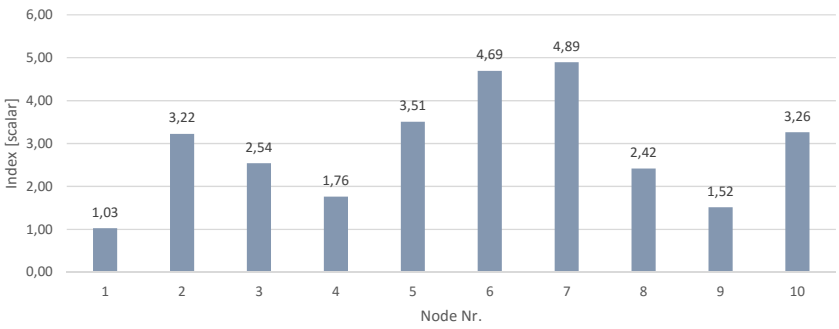

(b) Index value at moment of maximum loadability

Figure 6.5: Indicator values at moment of maximum loadability after a gradual load increase

From figure 6.5 it can be seen that at the instant of maximum loadability, the method predicts correctly which node voltage collapse occurs at. There can be seen some steady state noise for certain indexes. This is most likely due to the ambient noise at certain loads accounting for a higher % of the load as they are smaller and the same amount of noise is present. The same noise is present through the whole simulation and it can be seen that as voltage collapse gets closer, the load noise has a less impact on the index.

6.3.1.1 *Effect of Variations in k on Convergence*

The convergence of the Thévenin impedance in the CT-method has been found to be largely dependent on two important factors, the direction of E_{th} and step size. The change in load and Thévenin impedance between consecutive measurements chooses the direction the algorithm takes, while the step length is chosen as the smallest of the three values given in equation 6.1.

$$\epsilon_E = min(\ \epsilon_{inf}, \epsilon_{inf}, \epsilon_{lim}\ ) \tag{6.1}$$

$$\epsilon_{inf} = |\ E_{th}^{i-1} - V_L^i\ | \tag{6.2}$$

$$\epsilon_{sup} = |\ E_{th}^{i-1} - E_{th}^{max}\ | \tag{6.3}$$

$$\epsilon_{lim} = |\ E_{th}^{i-1} \times k\ | \tag{6.4}$$

Mostly equation 6.4 will be the smallest of the three values, therefore large importance is put on the choice of the k parameter. In figure 6.6, the effect of varying k in a simulation with ambient load noise is shown.

As can be seen from in figure 6.6 a larger k gives faster convergence, but is more subsceptible to load changes. From testing, it is found that a k between 0.005 and 0.0001 gives good overall results for all the nodes. In scenarios where the system impedance changes in an instance, like line contingencies, a fast reaction time with a larger k is to be preferred.

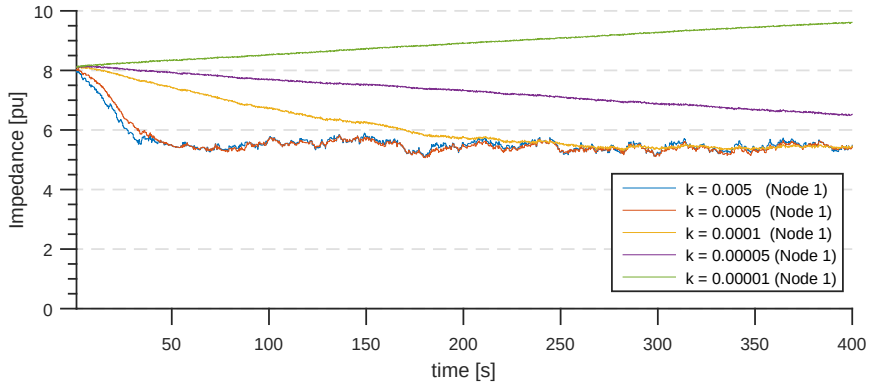

Figure 6.6: Effect of varying the parameter k, in the CT-method

6.4 DELTA METHOD

The Delta method uses two consecutive measurements of current and voltage to determine the Thévenin impedance of a system viewed from a node, therefore convergence time is not an issue as it is with the CT-method. If the following assumptions are made between two measurements, $E_{th} = const$ and $Z_{sys} = const$, the algorithm finds the real thevenin impedance directly. In figure6.7 the Delta method is tested on the same simulation as the CT-method with ambient load noise to determine the Thévenin impedance.

From figure 6.7 it can be seen that the Delta method does not show promising results in its estimate of the Thévenin equivalent. Compared to the true impedance seen at node 1 of $\approx 5.4\ [pu]$ there is a clear deviation of around $2.5 - 3\ [pu]$. A rate of change filter, $\Delta I > constant$, is also implemented for the best possible results. This way of filtering does have problems associated with it. When there are small changes in load power, as in figure 6.7, the constant which determines the change has to be small, in order to reevalute the Thévenin impedance if small changes occur. If the changes are large like in figure 6.8, a small constant will give a large amount of noise when the load starts increasing.

In figure 6.8 the load at node 1 is again subjected to a load increase after a fixed amount of time with only ambient load noise. The maximum loadability of the load occurs at $t = 363.5\ [s]$, while the Delta method

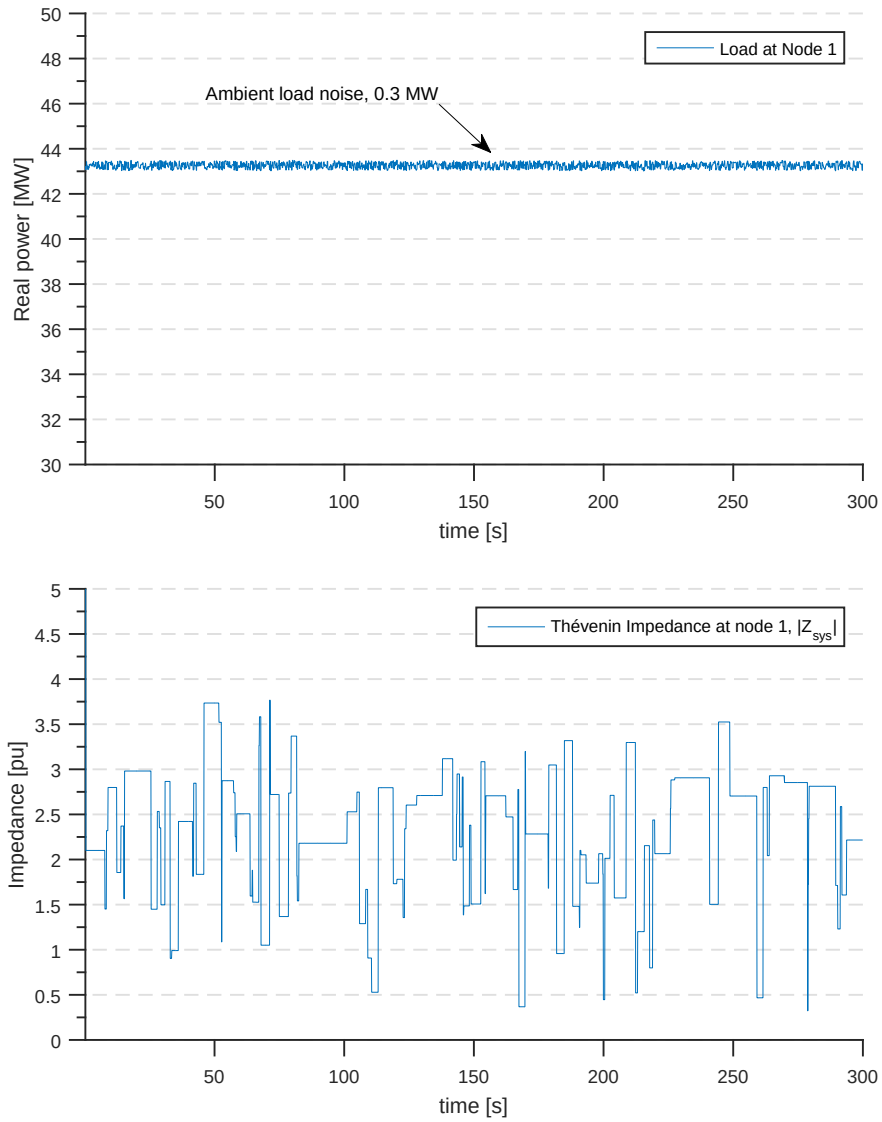

Figure 6.7: Delta methods performance in the presence of ambient load noise

predicts instability at $t = 377.5\ [s]$. It should also be noted the amount of noise around the occurrence of maximum loadability.

A few things can be done to improve this method. The addition of additional measurements by using a least squares method and cumu-

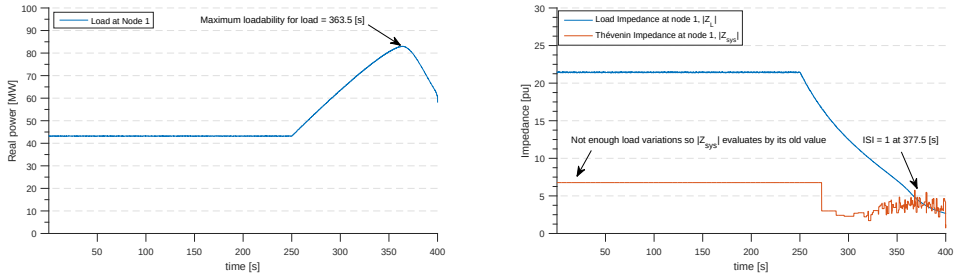

Figure 6.8: Estimating maximum loadability after a gradual load increase using the Delta method

lative filter as in [30] could be used to improve the performance of the method. An increased sampling time may also give better results, but the further between each sample the less likely it is that the assumptions about E_{th} and Z_{sys} will hold.

6.5 DUONG-UHLEN METHOD

The Doung-Uhlen method uses information about load power and topology to obtain the Thévenin impedance for a given node. In this section it is chosen to focus on four load buses, node 1, node 2, node 4 and node 8. An important part of this method is the modelling of boundary nodes. In this report, boundary nodes are tuned such that the load impedance at node 1 crosses the Thévenin impedance at the instant of maximum loadability as shown in figure 6.9.

The topology based Duong-Uhlen gives a steady estimate of the Thévenin impedance compared to the measurement method where the Thévenin impedance contains a large amount of noise. The ambient load noise and change in load power at node 1 has nearly no effect on the Thévenin impedance. In figure 6.10, the same scenario is run with indicators at four nodes in the system.

Compared to the measurement based method, the topology based Doung-Uhlen method gives reliable Thévenin estimates for the loads at the outer region of the study area. It can be seen that node 8 does have an

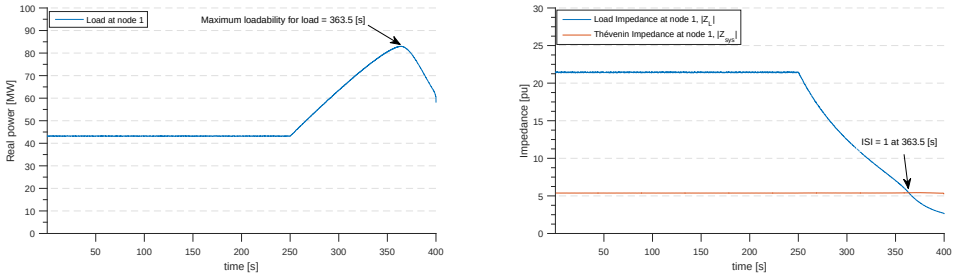

Figure 6.9: Estimating maximum loadability after a gradual load increase using the Duong-Uhlen method

unexpectedly large index value. This might be due to the node being closer to a boundary node and therefore being more affected by the modelling of the boundary nodes. The simplified method used in this report has also put a larger requirement on computing power. This can be optimized, and might therefore not pose as a problem in a real time implementation.

6.6 VIRTUAL IMPEDANCE METHOD

The virtual impedance as a method assumes observability of the whole power system unlike the Duong-Uhlen method that uses the fact that voltage stability can be considered a local problem, and can therefore be bounded. Since the power system in this report, the Norwegian transmission grid, is considered too large in order for a method that requires information about the whole system to be used, the boundary selection used in the Duong-Uhlen method is tested using the virtual impedance method.

As can be seen in figure 6.11 the method does not give satisfactory results. The system impedance at all the nodes except node 4 gives a too large estimate on the Thévenin impedance. A large contribution from the virtual impedance $\bar{Z}_{cj}$ can also be seen during the load increase at 400 $[s]$. As the change in load at node 1 should not give a contribution to a change in the Thévenin impedance at node 1, this term gives results

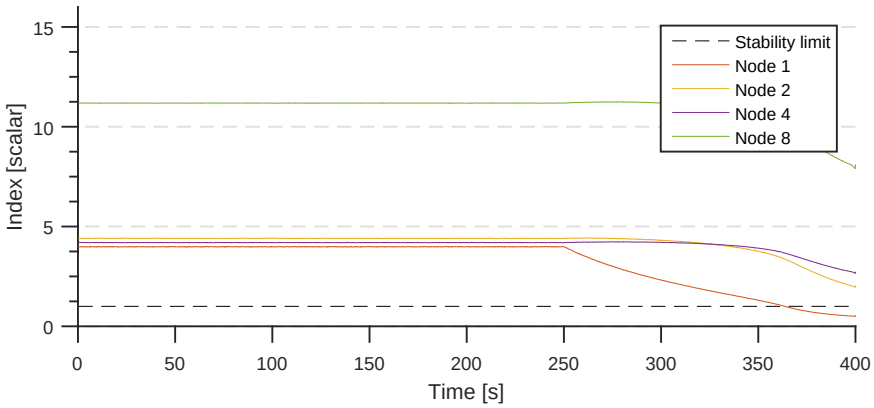

(a) Indicator values

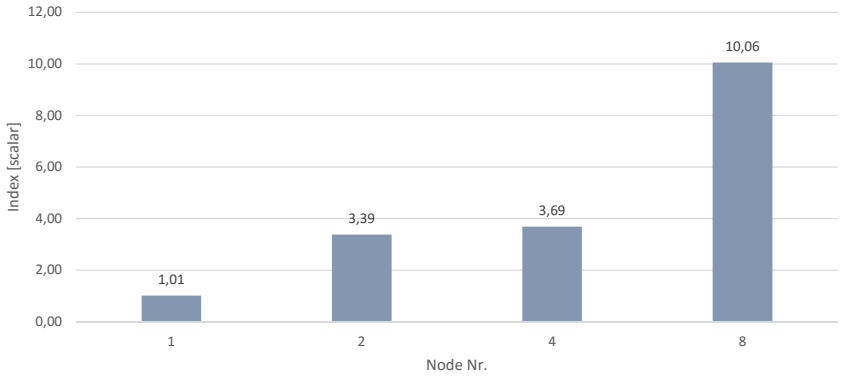

(b) At maximum loadability

Figure 6.10: Assessing the performance of multiple indicators using the Duong-Uhlen method

that are not realistic. In addition to this, during the inversion to find $\bar{Z}_{LL}$, the resulting answer gives negative impedances at the diagonal. This impedance which represents the transmission grid, gives a too large contribution than what is considered to be realistic. In conclusion the method might work with the constrained topology, but that result was not achieved in this thesis. Further study has to be done to give any definite answers to this.

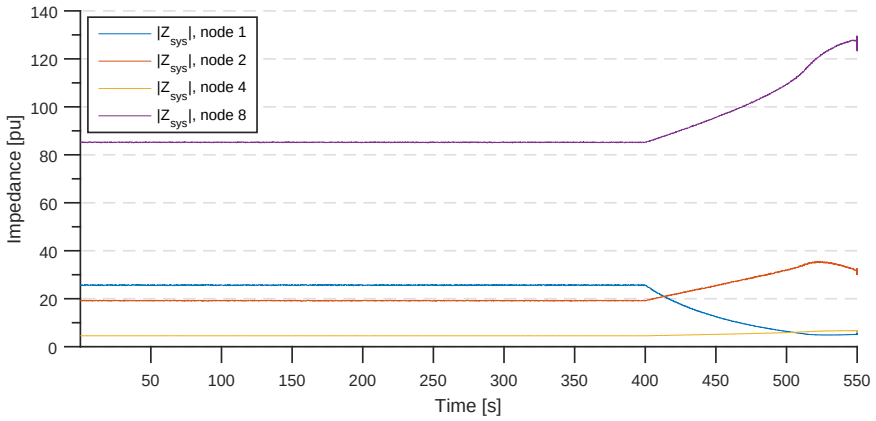

Figure 6.11: Performance of the virtual impedance method

6.7 SUMMARY

The performance of the different indicators have been tested. Two methods stand out in their performance, the local measurement based CT-method and the topology based Duong-Uhlen method. The measurement based CT-method is reliable and requires only a single PMU implementation for any given indicator. For the topology based Duong-Uhlen method, information about the load power and topology is required. However, signal noise is not an issue, which makes the method better for an emergency load shedding scheme if implemented properly.

7 CASE STUDY: LOFOTEN IN NORTHERN NORWAY

The goal of this thesis is to test the proposed emergency load shedding scheme in the Norwegian transmission system. The Lofoten region in Northern Norway is chosen as a case study since voltage stability previously has been a problem during high load winter periods. The operating scenario and model assumptions are presented in chapter 6. In this chapter, two different line contingency scenarios will be studied. In the first scenario, a single line contingency results in a slow decline in the state of the system eventually leading to voltage collapse. In the second scenario, two line contingences occurring at different time instances cause the system to become voltage unstable at a faster rate, demanding a fast response. The performance of the proposed emergency load shedding scheme for these scenarios will be tested.

7.1 CHOICE OF INDICATORS

In chapter 6 the performance of different indicators has been tested. From this, it has been obtained that the local CT-method and topology based Duong-Uhlen method are the two best performing indicators. The main method used in the presentation of results will be the CT-method, but the Doung-Uhlen method will be presented in certain scenarios to assess how it responds compared to the CT-method.

7.2 PLACEMENT OF INDICATORS

Based on the results presented in the performance assessment and general studies, four nodes have been chosen to be included in the proposed emergency load shedding scheme.

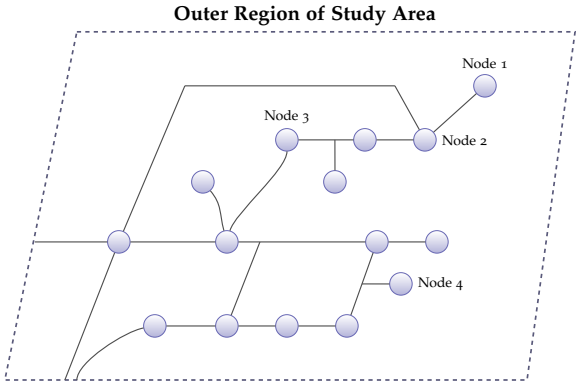

Figure 7.1: Indicator placement in the case studies

Three of the four chosen nodes are in the area where voltage stability is found to be the most problematic, node 1, node 2 and node 3. Node 4 is closer to a strong boundary node, but in certain contingent scenarios might reach its maximum loadability limit and become unstable. It also adds interesting comparison in scenarios where it should indicate that it is stable while the other nodes are reaching their loadability limit. The four chosen nodes are shown in figure 7.1

7.3 CASE 1: TRIP OF CRITICAL LINE

7.3.1 Operating Scenario

For this case an additional 35 $[MW]$, compared to an initial operating condition presented in chapter 6, is added to the load region. This is an unusual operating scenario, but changes in end-user consumption patterns that lead an unexpected rise in load demand has been the cause of previous voltage collapses, therefore the scenario is considered viable. With the additional loading, the area can be considered operating in a state defined as very stressed prior to any contingencies occurring.

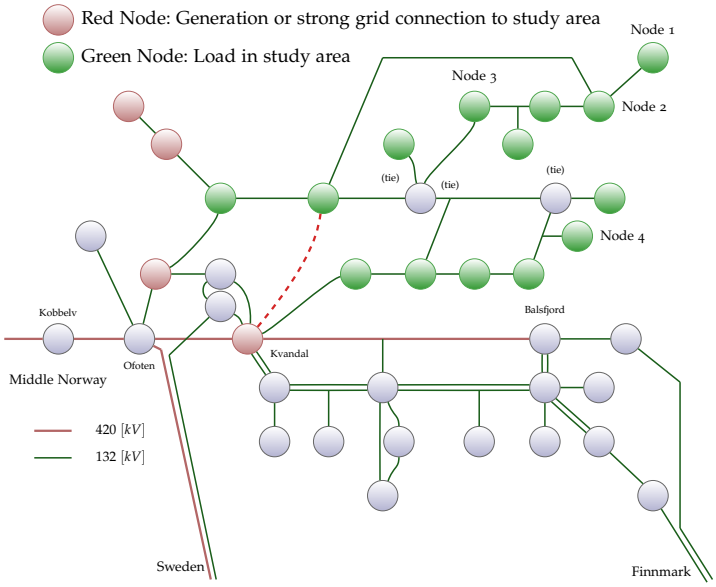

Figure 7.2: Case study scenario with trip of critical line

In figure 7.2 the scenario that has been studied in this section is illustrated. After 40 seconds the dashed line experiences an unexpected fault and gets disconnected. The results of the simulation are presented below.

7.3.2 Simulation Results

Due to the high load demand in this scenario, the initial voltages for the loads are quite low as shown in figure 7.3. At node 1, the voltage is as low as 0.9 $[pu]$, which implies a value of 117 $[kV]$ in a system usually operating above 130 $[kV]$.

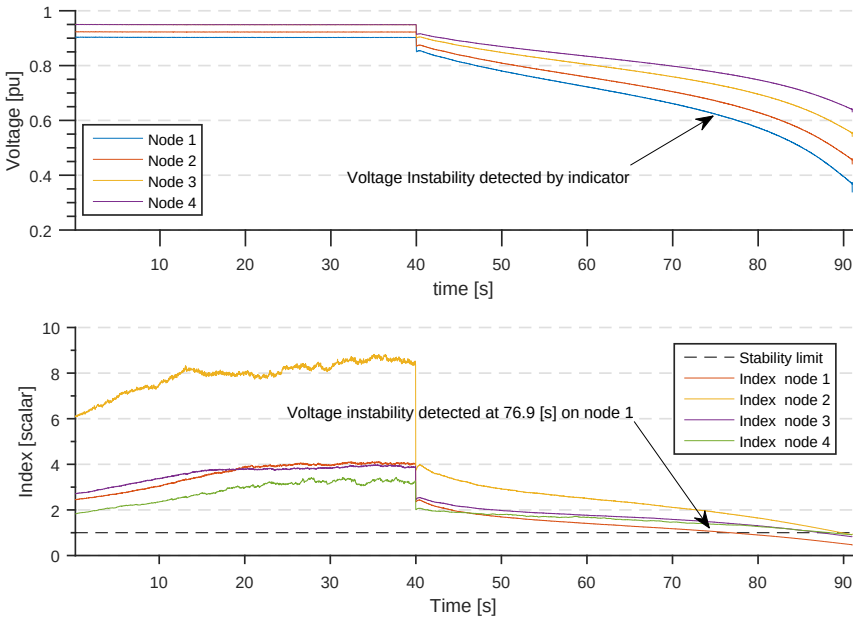

Figure 7.3: Voltage decline and indicator values after line contingency

After the line disconnection occurs at 40 $[s]$, the state of the system starts declining, and at 91 $[s]$ the system experiences a voltage collapse. From the initial line contingency there is a time window of 51 $[s]$ until the system collapses. The indicators detect instability at 76.9 $[s]$, and while the system has deteriorated considerably, as can be seen by the voltage profile, actions can be taken to restore the system.

7.3.2.1 *Mitigating Voltage Collapse*

Two approaches to load shedding was suggested in section 5.2.3 for the proposed emergency load shedding scheme. These two methods will

now be tested, and the effectiveness of each approach is evaluated.

In method 1 load shedding is initiated by either one of two criteria; an indicator stays below one ($ISI \leqslant 1$) for 3 $[s]$, or a rapid decline to $ISI = 0.9$ causes the system to initate load shedding immediately, without waiting for 3 $[s]$ to pass. Figure 7.4 shows an example where two rounds of load shedding has to be done prior to the restoration of the system. The initial round is triggered by $ISI = 0.9$ where 10 $[MW]$ is shed at node 1. For the second round, two scenarios are chosen to be studied. Either load shedding is initiated by the rules used for the initial load shedding, or load shedding is done the instant it crosses maximum loadability after load has been shed.

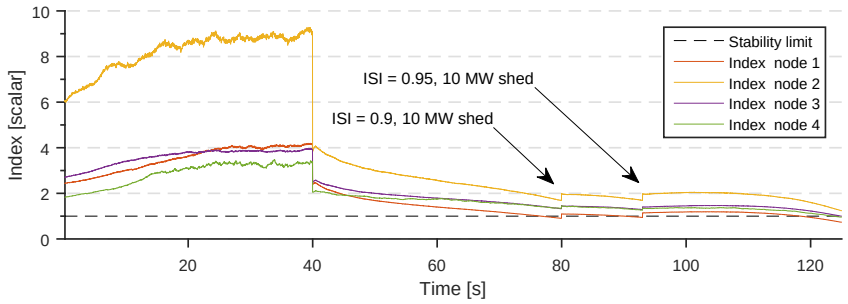

(a) Round two of load shedding initiated at $ISI = 0.95$ (value after 3 seconds)

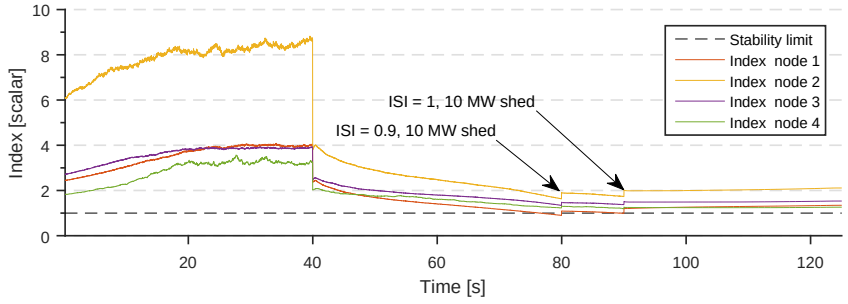

(b) Round two of load shedding initiated at $ISI = 1.0$

Figure 7.4: Initiating round two of load shedding based on different rules

As can be seen from figure 7.4 the time at which load shedding occurs is of great significance. A time delay of 3 seconds when shedding the

same amount of load is the difference between the system remaining stable or a voltage collapse occurring.

From this it can be seen that the indicator indicates voltage collapse, and by using its available mitigation resources a voltage collapse can be avoided. It should be noted that even though the system is stable after the initial load shedding, it is still in a critical state, and actions need to be taken to restore the system to a stable operating point.

In method 2, load shedding is initiated by the same two criteria as in method 1, but the amount of load to be shed is calculated by:

$$P_{shed} = P^i \times (1 - ISI^i) \times k$$

Using the same scenario, load shedding is initiated initially when the $ISI = 0.9$. From this, a value for the amount of load shed is calculated by measuring the load power at the time instance the load shedding occurs:

$$P_{shed} = 44[MW] \times (1 - 0.9) \times 4 = 17.6\ [MW]$$

As the loads can only be disconnected in instances of 10 $[MW]$, and up to 20 $[MW]$, the methods round up in value to assure that enough load is shed. Therefore, using the second method, 20 $[MW]$ is shed instantly. This is shown in figure 7.5

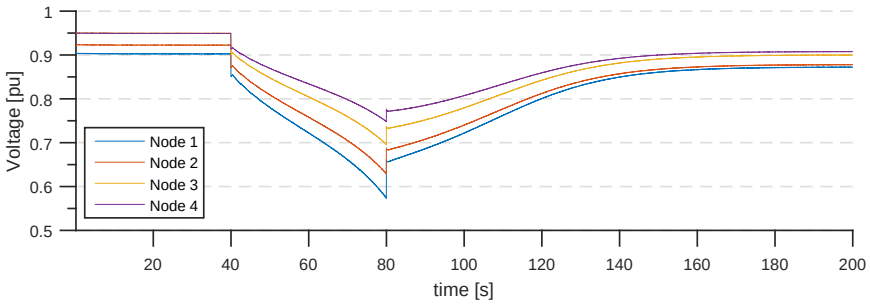

(a) Voltage after 20 $[MW]$ is shed at node 1

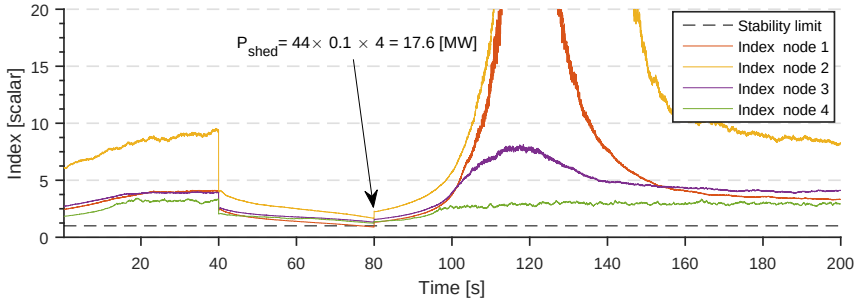

(b) Indicator values after 20 $[MW]$ is shed at node 1

Figure 7.5: Initiating round two of load shedding based on different rules

As can be seen in the figure, the system instantly regains stability, but there is some strange behaviour exhibited by the indicator after the load is shed. This might be a result of the load restoration causing the indicators to estimate the Thévenin incorrectly. With the same scenario using the Duong-Uhlen method, a significant improvement in the behaviour of the indicators after the load has been shed can be seen. This is illustrated in figure 7.6.

Considering the course of action and the importance of time at which load shedding occurs, the more aggressive response of shedding 20 $[MW]$ initially is to be preferred. In figure 7.4 it is shown that the margins determining whether the system stabilises or collapses are quite small. In a real system with measurement error and other uncertainties, the

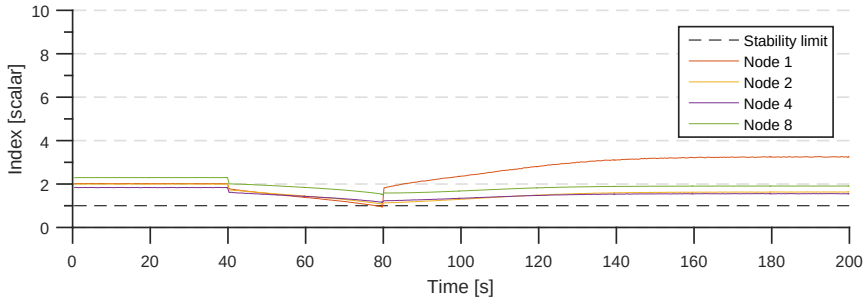

Figure 7.6: Steady state Indicator Stability Index values with the CT-method

approach of operating at safe values is always preferable to the system collapsing.

7.4 CASE 2: TRIPPING OF TWO LINES AT DIFFERENT TIME INSTANCES

7.4.1 Operating Scenario

For this case, a lighter loaded situation in the Lofoten region is chosen. The total loading in the study area is 300 $[MW]$, which is 40 $[MW]$ less than the considered base case in chapter 6. The situation presented in this case is a common occurrence during winter months. It is a relatively stable operating condition, where the system is able to withstand the contingency used in the first case study without losing system stability.

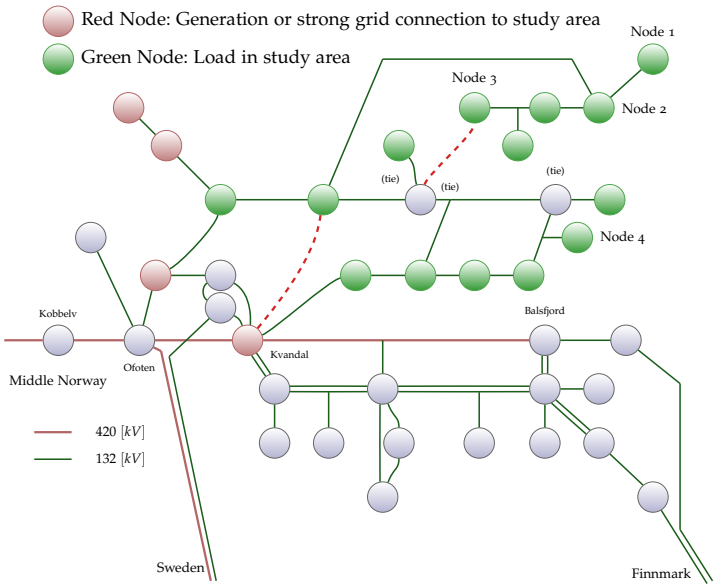

Figure 7.7: Steady state Indicator Stability Index values for case 1

In figure 7.7 the studied scenario in this section is illustrated. After 20 seconds the dashed line connected to Kvandal experiences an unexpected fault and gets disconnected. Following this, another transmission line experiences a fault at 80 seconds, causing the outer study region to lie on a radial. The power flow over the radial line connected to node 2 can cause the line to be disconnected by overcurrent relays,

prior to the system experiencing a voltage collapse. However, as the situation is interesting for studying voltage stability, it is assumed that the rating of the transmission line is high enough so the operating condition imposed by the second fault can be considered valid.

7.4.2 Simulation Results

With the lighter load demand, the simulation almost matches the orginal case, prior to the disconnection of small scale generation. It is therefore characteristic of a winter day around Lofoten, and it can be seen that the voltage profile is considerably better than in the previous simulation. All the measured voltages lie above 1 $[pu]$ or, 130 $[kV]$ as is usual in day to day operation of this part of the power system.

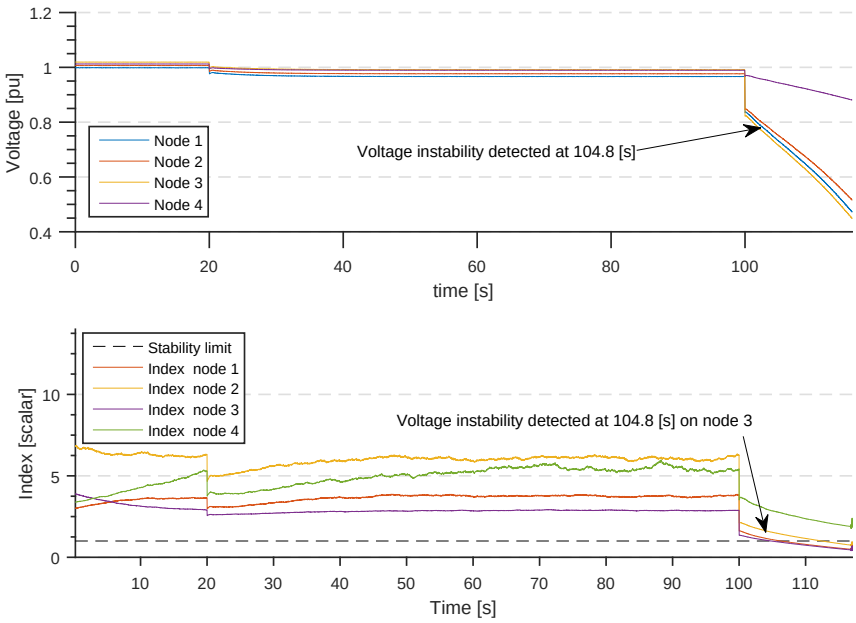

Figure 7.8: Indicator Stability Index values for two methods of load shedding in case 2

Following the first contingency, a small drop in voltage is observed at all the buses, and they settle at this operating point. Without the reconnection of the transmission line, the system is now operating in

an insecure state, and when the second line is disconnected at 100 $[s]$, the state is worsened rapidly until voltage collapse occurs at 117 $[s]$, as shown in figure 7.8.

7.4.3 Mitigating Voltage Collapse

As in the previous study case, two approaches to load shedding are tested. After the second line contingency, the situation is more severe than the previous case. Within 17 $[s]$ of the second fault, the system collapses, leaving less time to perform corrective actions. Unlike the previous scenario, voltage instability is first detected at node 3, which is assumed correct behaviour as the highly loaded node now lies at the end of a radial.

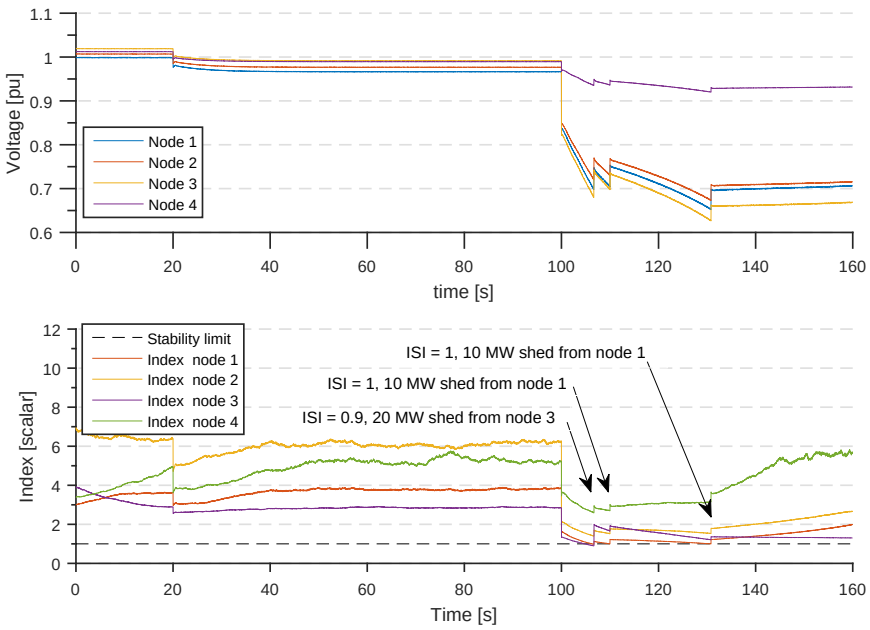

Figure 7.9: Voltage and indicator values using a modified method 1 for load shedding

Using method 1 directly is too conservative for the given scenario, therefore a modified version that disconnects 20 $[MW]$ when the Impedance Stability Index is equal to 0.9 has been used. As can be seen in figure

7.9, the initial shedding of 20 $[MW]$ is not enough. After the initial load shedding, the indicator at node 1 indicates that it has reached its loadability limit. This happens two times in a row, with 10 $[MW]$ being shed at each instance. After a total of 40 $[MW]$ being disconnected, the system regins stable operation.

Using method 2 with the same constant, k, as used in case 1 does not return the system to a stable operating condition. As the case is so severe, the emergency load shedding scheme has to completely disconnect one of the two feeders connected to the substation at node 3. The choice ends up being the 22 $[kV]$ which has a load demand of 30 $[MW]$. In general, a preferable choice is to use the feeder where the industry end-users are connected. This is usually at the 66 $[kV]$ level, meaning that if a disturbance occurs where a complete load has to be disconnected, the 66 $[kV]$ feeder can be preferable. This claim does not always hold, and therefore investigation prior to the implementation of such a scheme has to be done.

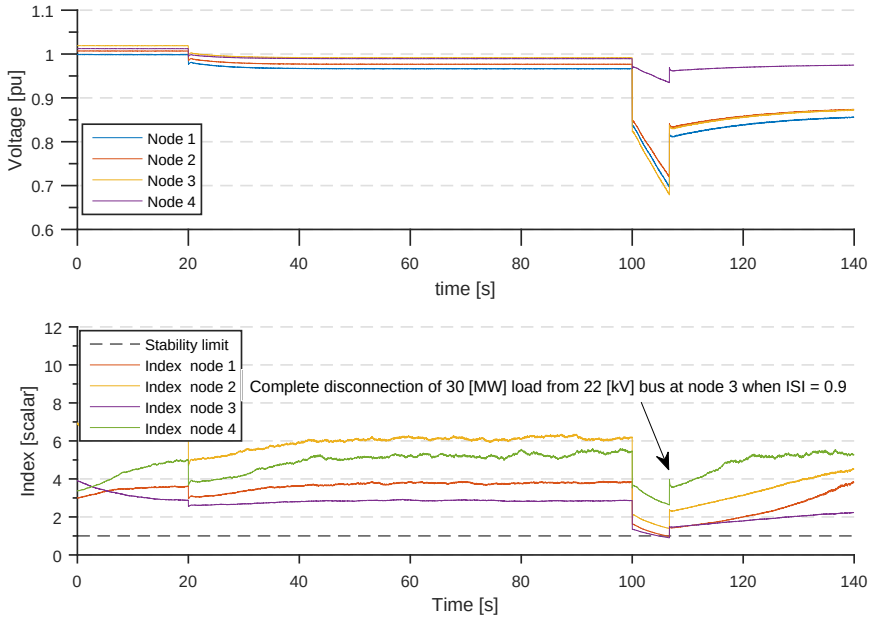

Figure 7.10: Voltage and indicator values using a modified method 2 for load shedding

8 DISCUSSION

This chapter discusses and summarises the findings from chapter 6 and 7.

8.1 VOLTAGE STABILITY INDICATORS

Out of the four presented indicators, the Corsi-Taranto method and Duong-Uhlen method perform well under all the scenarios used in the study cases. The measurement based Delta method, while easy to implement, is very sensitive to noisy signals, which makes the method unsuitable for applications where robust indicators are required. An implementation of the virtual impedance method was also done using the same boundary selection as the Duong-Uhlen method. The method did not give correct results. It is not known if the boundary selection does not work with the given method, or if there are mistakes made in the implementation. As the Delta method and virtual impedance method do not show promising results, they have not been taken into consideration in the emergency load shedding scheme.

In the studies done in 6 the Corsi-Taranto and Duong-Uhlen methods show that they are able to detect when a load reaches its maximum power transfer, often referred to as the tip of the nose point. This has been tested by a gradual load increase at a monitored node. This is expanded upon in chapter 7, were the system is subjected to two different line contingencies where voltage collapse occurs fast and slow, respectively. When a transmission line is disconnected, the impedance of the system increases, which both of the methods correctly show. The topology based Duong-Uhlen method handles the transient behaviour

during contingencies and load shedding well, but as the boundaries are considered static for the case of simplicity in this report, and dynamics are present, there is error in the estimate of the Thévenin impedance.

The CT-method shows good convergence qualities in most of the situations it has been applied. A few observations have been made for the steady state performance of the CT-method in section 6.3.1. The reason for this may be that there is negligible amounts of reactive power flowing towards the load at steady state operation. As the system is close to voltage instability, the loads draw larger amounts of reactive power. Therefore, the CT-method detects voltage instability better close to voltage instability. In this regard, it almost detects voltage instability as well as the Duong-Uhlen method.

Some convergence issues are also presented in 7.3.2.1 after load shedding is initiated. The ISI first increases in value and then decreases before settling at a steady state value, as shown in figure 7.5. A reason for this might be due to the restoration of the loads. However, even though the algorithm struggles in this situation, no false triggers of instability are observed.

Implementing the Corsi-Taranto method only requires a single phasor measurement unit at the monitored load. In contrast, the Duong-Uhlen method requires information about load powers from SCADA as well as information about topology. With the current SCADA system these measurements are updated every 10 seconds, and as shown with the scenario in section 7.4, the system collapses within a time frame of 17 seconds. With data acquisition only every 10 seconds, these measurements are not acquired by the SCADA system fast enough, giving a false estimation of the Thévenin equivalent. In addition, PMU measurements are needed at boundary nodes as well as the monitored load. As more measurements and information is used, the system therefore is harder to maintain operational.

8.2 PERFORMANCE OF THE PROPOSED EMERGENCY LOAD SHEDDING SCHEME

A proposed emergency load shedding scheme is tested using two different scenarios where both fast and slow dynamics are present. In these studies, the proposed emergency load shedding scheme has shown room for improvements. The predefined limits for when load shedding should be initiated are quite low, leaving the system in a critical state prior to any load being shed. This has resulted in an operating scenario where other relays might act prior to load shedding being initiated. To improve these limits, more studies have to be done to assess what is defined as a critical state in the system.

The time at which load shedding is initiated has also proved to be crucial. For the studied scenarios, the same amount of load or more had to be shed in the instances where multiple rounds of load shedding was used as opposed to when a single larger amount was shed. The larger amount also put the rest of the system in a healthier state post load shedding. As there is a direct connection between the ISI value and the time at which load shedding occurs, a larger ISI value to initiate the load shedding is preferred. The set point of these predetermined rules are of even more importance if induction machines are present in the system. These types of machines can stall, causing the system to become even more unstable.

An important observation is that the slower dynamics gave better results for the proposed emergency load shedding scheme. A fast deterioration of the state of the system makes the proposed type of load shedding in multiple stages inefficient, as the system deteriorates faster than the improvements made by shedding load. This can cause either a voltage collapse, or force a larger amount of load than necessary to be shed, which is not desirable in a system that wants to keep the amount of load shed to a minimum.

8.3 VALIDITY OF RESULTS

The power system model provided by Statnett is not good enough when asssessing voltage stability for the studied area of the power system. Load modelling is an important part of voltage stability studies, and the response of tap changing transformers are not sufficiently represented using the current load modelling. In addition to this, the ZIP parameters need to be improved upon. These are important when considering a shorter time frame in the dynamics. The neighbouring country, Sweden, might also have given a larger contribution had it not been modelled as a constant load. This might however not be a significant contribution as it is quite far from the study region.

The overexcitation modelling needs to be further improved upon. Without measurements for the response of the generator in question, good modelling is hard to achieve. As overexcitation limiters are crucial when studying voltage stability, this needs to be taken into consideration.

As the small-scale generators in the study area had to be disconnected, a small contributor of active and reactive power in the study areas was removed. Although its contribution might not have been significant, it is shown that small contributions can be difference makers in whether their respective systems remain voltage stable or collapse. The potential tripping of these machines in fault scenarios can also contribute to worsen the state of the system.

Part IV

CLOSURE

9 CONCLUSION AND FURTHER WORK

9.1 CONCLUSION

Out of the studied indicators, the measurement based Corsi-Taranto method, and the topology based Duong-Uhlen method perform best in the studies they have been tested in. The methods were tested using a gradual load increase in the system, as well as studies where different line contingencies occured, resulting in both fast, and slow voltage collapse.

In implementation, the Corsi-Toranto method only requires a single phasor measurement unit, compared to the Duong-Uhlen method which requires load powers and topology information from SCADA, in addition to PMU measurement at boundry nodes and the monitored load. As the Duong-Uhlen method requires a large amount of measurements to be implemented, there is a larger chance that something goes wrong. The positive side of using the Duong-Uhlen method is that it is marginally affected by ambient load noise and disturbances occuring in the power system. In this, the Corsi-Taranto method shows less promising results, but as it is only based on a single PMU measurement the performance is considered good.

An Emergency Load Shedding scheme (ELS) is also proposed. Using a set of predetermined rules, load is shed when an indicator indicates that the system is unstable. The performance of the proposed emergency load shedding scheme is not ideal, but in most cases the system is restored to stable operation following contingecies. The time at which load shedding occurs has proved to be important. In this regard, more conservative limits could have been chosen, as it is shown that close to the nose point load restoration often causes the system to perform multiple instances of load shedding. An important observation is

that the system performs better when slower dynamics are present, or when the system gradually approaches voltage collapse.

9.2 FURTHER WORK

There are different continuations to this thesis that can be investigated.

1. In the measurement based Corsi-Taranto method, the assumption done in this report, that capacitive loads can be modelled as inductive loads, needs to be further studied. Based on the studies done, the assumption gives promising results, but more tests has to be conducted to validate if the assumption holds.
2. The robustness of the indicators needs to be further studied. In a real power system, short circuits occur, and the system is never completely balanced. There is also the response of non-linear components such as tap changing transformers which are modelled by a smoother response in this report. To test the proposed algorithms, a monitored test should be conducted using real PMU measurements.
3. Load modelling is of great importance, and in the presence of dynamic loads the time at which load shedding occurs need to taken into consideration. In this report a fixed time delay is used in the proposed emergency load shedding scheme. It is shown in chapter 7 that different scenarios greatly impact the time at which a voltage collapse might occur. An increased amount of wind power can lead to more induction machines. Therefore, stalling of machines should be taken into consideration.
4. The proposed indicators only give a margin until voltage collapse, and no information about when it might occur. Methods where voltage instability is detected before the system is degraded are proposed, but usually require good system observability. Further studies should be done on methods using measurement available currently or in the near future, in order to indicate when a collapse might occur.
5. To minimize the energy not supplied, further study should be done on the amount of load required to restore a system. Many methods propose formulating the problem as an optimization problem. This can be a good solution, but in most real cases

the load is not controllable to the degree that such a scheme is possible. If the optimization problem is well formulated and constrained such that it represents a real smart grid implementation, this can be an interesting study.

6. The details in the proposed emergency load shedding scheme needs to be looked closer into. As of now, the levels where a warning is issued and load shedding occurs are not derived scientifically. These levels are critical as to how the scheme responds. Too conservative estimates may lead to accidental load shed in the system, and too small limits may cause the system to collapse.

Part V

APPENDIX

A MATPOWER

In the topology based method, matpower was used as a tool to get the admittance matrix. Matpower [39] and PSS®E are very similiar in the structure of the program and the way models are built. PSS®E models can also be directly converted into Matpower files. A brief summary of the usage of Matpower in this report is given below.

First a model of the admittance matrix has to be built,

```
function mpc = matpower_topology( y1 , i * sp , S_1 , S_2 , S_3 , k)

%% MATPOWER Case Format : Version 2
mpc.version = '2';

%%----- Power Flow Data -----%%
%% system MVA base
mpc.baseMVA = 1000;


%% Specify channels PSS\E for Gs and Bs


%% bus data
%
% It is important to add channels for loads to Gs and Ps as the admittance matrix built
% in matpower is used for powerflow. Therefore loads should be modelled as shunts.
% An alternative approach is to modify makeYbus
% Care should be taken in the direction of power flow
%
% bus_i type  Pd  Qd      Gs              Bs      area Vm  Va  baseKV  zone  Vmax  Vmin
mpc.bus = [
   1    1    0 0 Real power (MW)    Reactive power (Mvar)  1    1 0 130    1    1.3    0.8;
   2    1    0 0 Real power (MW)    Reactive power (Mvar)  1    1 0 130    1    1.3    0.8;
   3    1    0 0 Real power (MW)    Reactive power (Mvar)  1    1 0 130    1    1.3    0.8;
   4    1    0 0 Real power (MW)    Reactive power (Mvar)  1    1 0 130    1    1.3    0.8;
   5    1    0 0 Real power (MW)    Reactive power (Mvar)  1    1 0 130    1    1.3    0.8;

];

%% generator data
%
mpc.gen = [
% Not relevant when building the admittance matrix
]
%% branch data
%
% Here fbus tbus    r      x      b  are important to specify
%
% fbus   tbus     r      x      b     rateA rateB rateC     ratio angle status  angmin  angmax
mpc.branch = [
from bus   to bus   R in pu     X in pu    0    999   999    999     0    0       1    -360   360 ;
from bus   to bus   R in pu     X in pu    0    999   999    999     0    0       1    -360   360 ;
from bus   to bus   R in pu     X in pu    0    999   999    999     0    0       1    -360   360 ;
from bus   to bus   R in pu     X in pu    0    999   999    999     0    0       1    -360   360 ;
];
```

To create Y_{bus} and Z_{bus}

```
S_1 = boundry power flow;
S_2 = boundry power flow;
S_3 = boundry power flow;

% y1 is outfile from PSS\E converted to be read in matlab
% sp is sampling rate

k = 1;

%
for i = 1 : j
      % Calling the function where Ybus is
          sornettet = matpower_topology( y1 , i * sp , S_1 , S_2 , S_3 , k);
          % Creating Ybus
          [ yb , ~ , ~ ] = makeYbus( sornettet );
          % Inverting to get Zbus
      Z_th = inv ( yb);
      Zth( 1 , i ) = Z_th ( 1 , 1 ) ;

end
%% After fault occurs call a modified Ybus without the disconnected line
% this can be done in one loop but for simplicity is chosen to be done in two
for i = j : end
          sornettet = matpower_topology_mod( y1 , i * sp , S_1 , S_2 , S_3 , k);
          [ yb , ~ , ~ ] = makeYbus( sornettet );
      Z_th = inv ( yb);
      Zth( 1 , i ) = Z_th ( 1 , 1 ) ;

end
```

What is shown in this part of the appendix is a limited set of the method use. As most of the data is considered sensitive, care has been taken in the presentation and only a general outline for the usage of matpower to find the Thévenin equivalent impedance is presented.

B MODEL DATA

B.1 DYNAMIC LOAD MODELLING

The load model used is the EXTLAR type found in the PSS®E documentation [2]. The structure of the model can be seen in figure B.1.

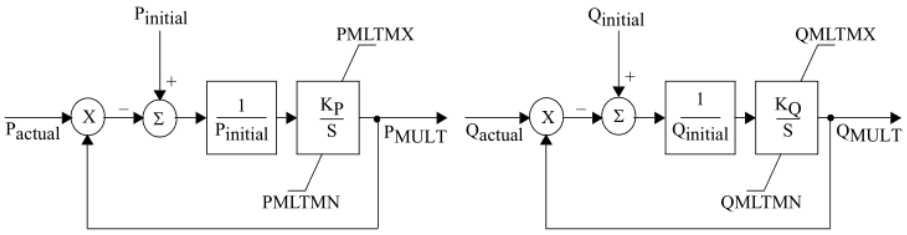

Figure B.1: Block diagram of the EXTL model from PSS®E documentation [2].

EXTLAR is an area specific implementation, therefore no individual load specification had to be done. Parameters were chosen based on previous work done by Vegar Storvann [1]. The full list of parameters can be found in table B.1

K_p	PMLTMAX	PLMTMIN	K_Q	QLMTMAX	QLMTMIN
0.3	100	0	0.3	100	0

Table B.1: Parameter list for the EXTL model implemented.

B.2 OVEREXCITATION EXCITATION LIMITER

To model the overexcitation limiters the, MAXEX2 model from the PSS®E is used. Time constants and parameters were chosen based on generators with similar nominal power output.

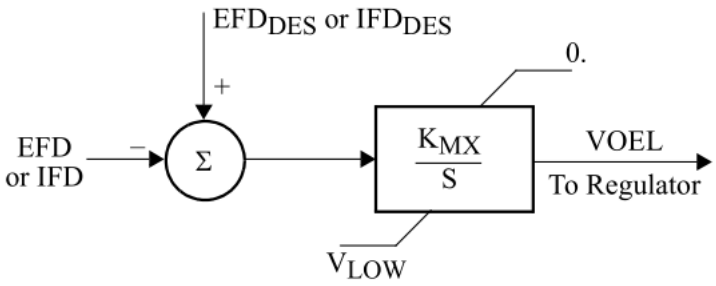

Figure B.2: Block diagram of the MAXEX2 model from PSS®E documentation [2].

Parameter	Value
EFD_{RATED} (pu)	2
EFD_1 (pu of rated)	1.1
$TIME_1$ (s)	180.0
EFD_2 (pu of rated)	1.4
$TIME_2$ (s)	30.0
EFD_3 (pu of rated)	2
$TIME_3$ (s)	10.00
EFD_{DES} (pu of rated)	1.1
K_{MX}	0.100
V_{LOW} (pu)	0.1

Table B.2: Parameter list for the MAXEX2 model implemented.

BIBLIOGRAPHY

[1] V. Storvann, "Maintaining Voltage Stability," Master's thesis, NTNU, 2012.

[2] S. E. Inc. and S. P. T. International, "PSS ®E model library, 32.05," 2010.

[3] "IEEE Task Force on blackout Experiences and Lessons, Best Practices for System Dynamic Performance, and the Role of New Technologies," *ResearchGate*, July 2007.

[4] C. D. Vournas, G. A. Manos, J. Kabouris, and T. V. Cutsem, "Analysis of a voltage instability incident in the Greek power system," in *IEEE Power Engineering Society Winter Meeting, 2000*, vol. 2, pp. 1483–1488 vol.2, 2000.

[5] C. D. Vournas, V. C. Nikolaidis, and A. A. Tassoulis, "Postmortem analysis and data validation in the wake of the 2004 Athens blackout," *IEEE Transactions on Power Systems*, vol. 21, pp. 1331–1339, Aug. 2006.

[6] "Generally Accepted Reliability Principle with Uncertainty modelling and through probabilistic Risk assessment, D1.1 State of the art on reliability assessment in power systems." http://www.garpur-project.eu/deliverables, 2014.

[7] "Continental Europe Operation Handbook." https://www.entsoe.eu/publications/system-operations-reports/operation-handbook/, 2004.

[8] P. Kundur, J. Paserba, V. Ajjarapu, G. Andersson, A. Bose, C. Canizares, N. Hatziargyriou, D. Hill, A. Stankovic, C. Taylor, T. Van Cutsem, and V. Vittal, "Definition and classification of power system stability IEEE/CIGRE joint task force on stability

terms and definitions," *IEEE Transactions on Power Systems*, vol. 19, pp. 1387–1401, Aug. 2004.

[9] C. V. Thierry Van Cutsem, *Voltage Stability of Electrical Power Systems*, vol. 19.

[10] "FoU i Statnett." www.statnett.no/Global/Dokumenter, 2015.

[11] B. M. Kjetil Uhlen, Philip Overholt and O. Valentine, "Synchrophasor applications for wide area monitoring and control," *ISGAN annex 6 power T&D systems*, 2016.

[12] J. De La Ree, V. Centeno, J. Thorp, and A. Phadke, "Synchronized Phasor Measurement Applications in Power Systems," *IEEE Transactions on Smart Grid*, vol. 1, pp. 20–27, June 2010.

[13] "WAMS (Wide Area Monitoring System)." www.gridtech.eu/events/12-technologies/23-wams-wide-area-monitoring-system, 2016.

[14] D. T. Duong, K. Uhlen, G. N. Taranto, and S. Lovlund, "A comparative case study of online voltage instability monitoring," in *PowerTech, 2015 IEEE Eindhoven*, pp. 1–6.

[15] D. T. Duong, K. Uhlen, and S. Lovlund, "A method for real time voltage stability monitoring in sub-transmission networks," in *Power Systems Computation Conference (PSCC), 2014*, pp. 1–7.

[16] J. Lavenius, L. Vanfretti, and G. N. Taranto, "Performance assessment of PMU-based estimation Methods of Thevenin Equivalents for real-time voltage stability monitoring," in *2015 IEEE 15th International Conference on Environment and Electrical Engineering (EEEIC)*, pp. 1977–1982.

[17] C. A. Canizares, F. L. Alvarado, C. L. DeMarco, I. Dobson, and W. F. Long, "Point of collapse methods applied to AC/DC power systems," vol. 7, no. 2, pp. 673–683.

[18] B. Otomega and T. V. Cutsem, "Undervoltage Load Shedding Using Distributed Controllers," *IEEE Transactions on Power Systems*, vol. 22, pp. 1898–1907, Nov. 2007.

[19] T. Amraee, A. M. Ranjbar, and R. Feuillet, "Adaptive under-voltage load shedding scheme using model predictive control," *Electric Power Systems Research*, vol. 81, pp. 1507–1513, July 2011.

[20] A. Mahari and H. Seyedi, "A wide area synchrophasor-based load shedding scheme to prevent voltage collapse," *International Journal of Electrical Power & Energy Systems*, vol. 78, pp. 248–257, June 2016.

[21] T. V. Cutsem, "An approach to corrective control of voltage instability using simulation and sensitivity," *IEEE Transactions on Power Systems*, vol. 10, pp. 616–622, May 1995.

[22] M. M. Begovic and A. G. Phadke, "Control of voltage stability using sensitivity analysis," *IEEE Transactions on Power Systems*, vol. 7, pp. 114–123, Feb. 1992.

[23] V. C. Nikolaidis and C. D. Vournas, "Design Strategies for Load-Shedding Schemes Against Voltage Collapse in the Hellenic System," *IEEE Transactions on Power Systems*, vol. 23, pp. 582–591, May 2008.

[24] M. Glavic and T. V. Cutsem, "Wide-Area Detection of Voltage Instability From Synchronized Phasor Measurements. Part I: Principle," *IEEE Transactions on Power Systems*, vol. 24, pp. 1408–1416, Aug. 2009.

[25] L. S. Vargas and C. A. Canizares, "Time dependence of controls to avoid voltage collapse," *IEEE Transactions on Power Systems*, vol. 15, pp. 1367–1375, Nov. 2000.

[26] N. G. Sakellaridis and C. D. Vournas, "Critical load-shedding time calculation based on region of attraction limits," in *Proceedings of 2010 IEEE International Symposium on Circuits and Systems*, pp. 529–532, May 2010.

[27] M. Begovic, B. Milošević, and D. Novosel, "A novel method for voltage instability protection," in *Proceedings of the 35th Annual Hawaii International Conference on System Sciences, 2002. HICSS*, pp. 802–811, Jan. 2002.

[28] V. Storvann, "Personal communication with Vegar Storvann, Statnett," 2015.

[29] "Standard load models for power flow and dynamic performance simulation," *IEEE Transactions on Power Systems*, vol. 10, pp. 1302–1313, Aug. 1995.

[30] L. Warland, *A Voltage Instability Predictor Using Local Area Measurements*. PhD thesis, The Norwegian University of Science and Technology Faculty of Electrical Engineering and Telecommunications Department of Electric Power Systems, 2002.

[31] S. Corsi and G. N. Taranto, "A Real-Time Voltage Instability Identification Algorithm Based on Local Phasor Measurements," vol. 23, no. 3, pp. 1271–1279.

[32] Y. Gong, N. Schulz, and A. Guzmán, "Synchrophasor-Based Real-Time Voltage Stability Index," in *2006 IEEE PES Power Systems Conference and Exposition*, pp. 1029–1036, Oct. 2006.

[33] S. R. James W. Nilsson, *Electric Circuits*, vol. 7.

[34] Y. Wang, I. R. Pordanjani, W. Li, W. Xu, T. Chen, E. Vaahedi, and J. Gurney, "Voltage Stability Monitoring Based on the Concept of Coupled Single-Port Circuit," *IEEE Transactions on Power Systems*, vol. 26, pp. 2154–2163, Nov. 2011. bibtex: wang_voltage_2011.

[35] G. N. Taranto, C. Oyarce, and S. Corsi, "Further investigations on a phasor measurement-based algorithm utilized for voltage instability awareness," in *Bulk Power System Dynamics and Control - IX Optimization, Security and Control of the Emerging Power Grid (IREP), 2013 IREP Symposium*, pp. 1–8.

[36] X. Mou, W. Li, and Z. Li, "A preliminary study on the Thevenin equivalent impedance for power systems monitoring," in *2011 4th International Conference on Electric Utility Deregulation and Restructuring and Power Technologies (DRPT)*, pp. 730–733.

[37] W. Li, Y. Wang, and T. Chen, "Investigation on the thevenin equivalent parameters for online estimation of maximum power

transfer limits," *Transmission Distribution IET Generation*, vol. 4, pp. 1180–1187, Oct. 2010.

[38] "Reaktiv Kompensering, Forbedret forsyningsikkerhet i Lofoten og Vesterålen."

[39] R. D. Zimmerman, C. E. Murillo-Sanchez, and R. J. Thomas, "MATPOWER: Steady-State Operations, Planning, and Analysis Tools for Power Systems Research and Education," *IEEE Transactions on Power Systems*, vol. 26, pp. 12–19, Feb. 2011.